Mineralisation in Layered Mafic-Ultramafic Intrusions

Hannah S. R. Hughes[1], Jens C. Ø. Andersen[1], Brian O'Driscoll[2]

[1]Camborne School of Mines, College of Engineering, Mathematics and Physical Sciences, University of Exeter, Tremough Campus, Penryn, Cornwall, TR10 9FE, UK
[2]Department of Earth and Environmental Sciences, University of Manchester, Oxford Road, Manchester, M13 9PL, UK

See Also: Economic Geology, Layered Intrusions, Igneous Rocks, Igneous Processes, Mining Geology, Mantle, Mantle Plumes, Minerals: Sulphides.

1. Introduction

Mineral deposits form in mafic-ultramafic layered intrusions (LMI) through a variety of magmatic processes. Chromium, platinum-group elements (PGE) and nickel (Ni) are almost exclusively extracted from mafic-ultramafic rocks (Table 1). LMI also host metals such as gold (Au), copper (Cu), cobalt (Co), vanadium (V), titanium (Ti) and scandium (Sc). Mafic-ultramafic rocks are major sources of dimension stone and aggregate, and increasingly, carbon capture and storage may generate significant demands for Mg-silicate (olivine and associated minerals).

Chromium, Ti and V are extracted from the oxide minerals chromite, ilmenite and titanomagnetite. Economic concentrations require several tens of percent of the host minerals, and exploration can therefore utilize remote sensing. Chromite is the only naturally-occurring source of Cr that can be economically extracted (Table 1). Vanadium is extracted from titanomagnetite and titanium from ilmenite (Table 1). In some mines, Fe is recovered as a by-product. Chromite forms exclusively in primitive mafic-ultramafic rocks, while titanomagnetite and ilmenite are more common in the evolved parts of LMI. In contrast to chromium, mafic-ultramafic igneous rocks are not exclusively the hosts of Ti and V resources. Vanadium is also extracted from black shale and crude oil, and titanium is concentrated in beach placers. Nickel, Cu, Co and the PGE associate naturally with sulphide minerals which normally occur in very low abundances in LMI. Sulphide mineralisation is commonly difficult to detect visibly – exploration is therefore dependent upon bulk geochemistry or assay and a sound understanding of igneous processes based on mineral chemistry.

Chromium, V and Ni are important alloying metals for steel production. Chromium and Ni provide corrosion resistance and are essential ingredients for stainless steel. Vanadium and Cr add hardness, strength and durability against fatigue, which is critical for the performance of steel tools, springs, bearings and gears. Platinum-group metals are used in jewellery. However, because most PGE are chemically (relatively) inert (except for Os), they are extensively used as catalysts for fuel emission reduction and in hydrogen fuel cells (Table 1).

2. Background Geology and Economics

2.1 Grades and Processing

Chromite ($FeCr_2O_4$) ore is mined at 20-50% chromite. Metallurgical chromite ore requires a concentrate with at least 30 wt.% Cr (44 wt.% Cr_2O_3), whereas refractory ore needs >60 wt.% (Al_2O_3 + Cr_2O_3) including >20 wt.% Al_2O_3 (Pohl, 2011). Following comminution (crushing and grinding), concentration is achieved by gravity and density methods (shaking tables and spirals) before mixing with a flux and smelting. The major product is ferrochrome (an alloy of Fe and Cr) that is directly used in stainless steel production.

Platinum-group metal ore is mined together with Ni, often with co-production of Cr, Cu, Co and Au. With the exception of Cr, these metals are hosted in solid solution in base metal sulphides (typically pentlandite, pyrrhotite, chalcopyrite) or as platinum-group minerals (PGM). The PGM are a diverse group of minerals, of which over 135 are known, including native metals, alloys and various other phases (including sulphides, arsenides etc; O'Driscoll and Gonzalez-Jimenez, 2016). Grades for PGE typically range between 1-10 g/t total PGE + Au, although high-grade deposits have values that might exceed 20 g/t. Nickel, Cu and Co grades are typically 0.5-3.0 wt.%, 0.1-2.0 wt.% and 0.05-0.1 wt.%, respectively. Mineral processing requires comminution and concentration (flotation and gravity) before pyrometallurgical and hydrometallurgical extraction, and refining.

Ilmenite ore is mined at around 15 wt.% TiO_2, which is equivalent to some 30 wt.% ilmenite (Charlier et al. 2006). Vanadium ore typically requires around 0.25 wt.% V_2O_5, although economic extraction is possible at lower grades where the metal is a by-product. The economic recovery of Ti and V, however, depends on many factors, notably how much Ti is locked into titanomagnetite and the extent to which titanomagnetite and ilmenite are intergrown. Mineral processing requires efficient separation of titanomagnetite from ilmenite, which initially requires magnetic separation (titanomagnetite is ferromagnetic, whereas ilmenite is paramagnetic). Vanadium may be processed into ferrovanadium,

63 which is used in the steel industry, or recovered as V_2O_5 through a roast-leach process. Titanium is
64 predominantly processed into white TiO_2-pigment for paint.

65 An overview of grades, ore minerals, products and uses for the main elements currently extracted
66 from LMI is provided in Table 1.

67

68 ***2.2 Magmatic Differentiation***

69 The formation of an ore deposit is the culmination of four key factors: *source*, *pathway*, *agent*, and
70 *deposition* (Fig. 1). In the case of ore deposits hosted within LMI, these factors are largely controlled
71 by magmatic differentiation processes, including partial melting, crystallisation, crustal
72 contamination, and immiscibility of coexisting melts (Fig. 1). Elements that are normally distributed
73 widely across a large volume and at low abundances must become concentrated into a small volume
74 to be amenable and economic for mining. Most of the elements that occur in mineralised deposits in
75 LMI are more abundant in the Earth's mantle (the *source*) than in the crust. Therefore ultramafic-mafic
76 magmas (commonly the *agent*) derived from partial melting of the mantle are relatively enriched in
77 these elements, compared to more felsic magmas from crustal source rocks. These ultramafic-mafic
78 magmas ascend from the mantle via conduits (*pathways*) to form crustal magma chambers. In these
79 chambers, progressive crystallization is accompanied by mineral settling which results in the
80 accumulation of mineral products (cumulates) at their base. Rocks in most LMI therefore generally
81 become successively younger upward through the magmatic stratigraphy, and the roof zones are
82 commonly eroded away. This process of fractional crystallisation means that magmas eventually
83 become saturated in mineral phases that might contain elevated abundances of economically
84 interesting metals (*deposition*). Crystallisation, either *in situ* or with some mechanical sorting,
85 facilitates the accumulation of minerals that may reach sufficient quantities to form a viable ore
86 deposit. Progressive crystallisation may also lead to the exsolution of immiscible liquids (sulphide or

Fe-rich silicate) and these have significant effects on the concentration and deposition of target elements. The unmixing of an immiscible liquid fraction from a magma may also be triggered by contamination of the crystallising LMI with crustal rocks.

The distribution of an element between coexisting phases and residual magma underpins the magmatic differentiation processes that concentrate metals from source to deposition. This includes the partitioning of an element between liquid magma and cumulus mineral (during the extraction of magma from the source region, or crystallisation from magma), or between coexisting liquids (silicate and sulphide magma). This is described as element partitioning and may be quantitatively expressed by the ratio of the concentration of element (*i*) in one phase to the concentration of *i* in the other phase. This ratio is termed the *Nernst partition coefficient* (*D*) such that:

$$D_i^{sulphide/silicate} = \frac{C_i^{sulphide}}{C_i^{silicate}} \quad [1]$$

Equation 1 is an example expressing *D* for element *i* between sulphide liquid and silicate magma, where *C* denotes concentration of *i*. If $D > 1$, then element *i* is said to be *compatible* and preferentially partitioned into sulphide liquid (in the case of Equation 1). For values of $D < 1$, *i* is *incompatible* into sulphide liquid and remains preferentially in the silicate magma. Whilst the partition coefficient may be used to numerically model trace element behaviour during partial melting and crystallisation, for the purposes of this chapter, *D* is used as an indication of an element's affinity for different magmatic phases (Table 1). The value of *D* effectively indicates the magnitude of this affinity.

This chapter will focus on the three main groupings of elements that may be mineralised within LMI: chromium (in chromite), Ti and V (in magnetite and ilmenite), and PGE-Ni (with minor amounts of Co, Cu and Au). Examples of exposures of mineralised LMI locations are also provided in Figure 2. Each of the following sections outlines the main minerals and mineralisation processes thought to operate in the formation of LMI. This chapter will therefore chiefly outline the mainstream models and

mechanisms thought to be in operation in LMI mineralisation, most of which are orthomagmatic. We will also discuss some high-temperature metasomatic and fluid-based processes, but acknowledge that some other models are beyond the scope of this short review.

3. Chromite

The rock type chromitite typically contains ≥ 60 vol.% chromite crystals, together with minor interstitial plagioclase, pyroxene and/or olivine. In LMI it forms seams and layers that range from < 1 mm to several meters thick (Mathez and Kinzler, 2016). LMI-hosted chromitites are one of Earth's main Cr repositories (Mungall and Naldrett, 2008; and references therein), and they are also associated with some of the largest PGE deposits. The formation of chromitite has been the subject of much debate in the petrological community (e.g., Boudreau, 2016; Latypov et al. 2013; 2017). A major problem is one of mass balance and specifically the question of how a trace element such as Cr (with abundances typically of 100-1000 ppm in LMI parental melts) can be concentrated to levels of 30-40 wt.% in metre-thick chromitite layers. An explanation is required for the observation that silicate magmas that mainly crystallise silicate minerals are able to precipitate only chromite as a liquidus phase during the formation of chromitite layers. The critical steps in forming LMI-hosted chromitite layers and are essentially controlled by the replenishment of the chamber by new magma. The relevant processes are described in the following sections by referring to both thick massive chromitite layers (tens of cm to metres thick) and thinner chromitite seams (mm to cm thick) in LMI.

3.1 Massive chromitite layers

Several massive chromitite layers occur in the Critical Zone of the ~2 Ga Rustenburg Layered Suite (Bushveld Complex) and the Peridotite Zone of the ~2.7 Ga Stillwater Complex (Cawthorn, 2015; Boudreau, 2016). The Kemi LMI in Finland also hosts a chromitite layer that reaches ~100 m thick in the centre of the intrusion. Massive chromitite layers generally formed in the lower portions of their

host LMI, where they appear to be intimately associated with the macro-scale rhythmic layering that developed in response to repeated additions of magma to the chamber. Massive chromitite layers developed systematically at the bases of cyclic units in the Bushveld and Stillwater Complexes (Fig. 3a). The layers are extensive and commonly of relatively uniform thickness along strike. As an example, the UG2 chromitite in the Bushveld Complex varies between ~0.4 and 2.5 m in thickness and can be traced continuously for 300 km across the Eastern and Western Limbs of the Bushveld Complex (Schouwstra and Kinloch, 2000). A thin (10-20 cm) 'leader' seam is systematically developed immediately above the UG2 chromitite, and thin (< 20 cm) chromitite seams also formed in the footwall rocks. These minor seams (above and below) locally merge and bifurcate with the main chromitite. In the UG2 layer, the chromitite has 75-90 vol.% chromite with interstitial plagioclase and pyroxene. Generally, the UG2 footwall comprises a pegmatoidal feldspathic pyroxenite, with locally developed anorthosite, and the hanging wall is made up of pyroxenite. One of the remarkable features of many massive chromitites of the Critical Zone (particularly well-expressed in the UG2 chromitite) is that they locally cut down through several metres of their footwall cumulates giving rise to structures referred to as 'potholes'. Potholes associated with the UG2 chromitite are circular or elliptical depressions (10 cm to 100 m wide and < 1-40 m deep) with gentle-to-steeply inclined sides that truncate the underlying layered rocks (Latypov et al. 2017a).

The formation of massive chromitite layers such as those in the Bushveld and Stillwater Complexes has been suggested to be triggered either by magma mixing (following the classic model of Irvine, 1977; Fig. 4a), by crustal contamination (Fig. 4a), and by pressure and/or fO_2 fluctuations. In the case of both the magma mixing and contamination mechanisms, the hybrid composition of the resultant magma becomes saturated in chromite only (Fig. 4a), leading to crystallisation of a monomineralic chromite layer as chromitite. Mondal and Mathez (2007), however, argued that the enormous amount of chromite in the UG2 layer must have involved the emplacement of magma that carried entrained chromite phenocrysts, with subsequent gravity-driven accumulation onto the magma chamber floor.

While this idea addresses the mass balance problem, more recent work by Junge et al. (2014) showed cryptic mineral compositional variations within the UG2 chromitite, that suggest it was constructed incrementally, rather than in a single 'event'.

In the Stillwater Complex, the association of chromitite with cyclic harzburgite-orthopyroxenite units has similarly been taken as evidence of chromite crystallisation in response to mixing of resident magma with repeated influxes of olivine-saturated (high-Mg) parental magmas (i.e., the mechanism outlined in Fig. 4a). Horan et al. (2001) used Os isotopes to argue for chromitite formation by mixing of variable proportions of a relatively primitive magma with one that had already seen crustal contamination. In a variant on this theme, Spandler et al. (2005) analysed chromite-hosted inclusions in the chromitites and proposed that assimilation of silica-rich country rock by the incoming magma forced the contaminated magma into crystallising chromite only, thereby forming the chromitite layers (Fig. 4a). Other suggestions include the crystallisation of chromite in response to pressure fluctuations in the magma chamber (Lipin, 1993) and hydration of magma to stabilise chromite as the only crystallising phase. Boudreau (2016; and references therein) discussed how hydration melting could work to produce the successive dunite/chromitite layers of the Peridotite Zone as restitic products of this process. This works by shifting the cotectic in the olivine-chromite-SiO_2 ternary phase diagram (Fig. 4b), expanding the chromite stability field such that the overall composition of the hybrid magma lies in the chromite-only field, and resulting in crystallisation of chromite alone with subsequent formation of the monomineralic layers by crystal settling or in situ crystallisation as for the mixing/assimilation model(s) (Fig. 4b).

3.2 Chromitite seams

Chromitite seams are typically a few millimetres to several centimetres thick and therefore uneconomic for chromium. Instead, the chromitite in the Merensky Reef (Bushveld Complex) is mined as one of the largest PGE deposits on Earth, highlighting the important association between chromitite

and PGE mineralisation in LMI. Similar to the massive chromitite layers, many seams formed directly at lithological contacts that preserve evidence of magma replenishment. The Merensky Reef chromitites formed between 20-400 m above the UG2 chromitite, close to the top of the transition between the Critical Zone and the Main Zone. Like the UG2, they are continuous around the Western and Eastern Limbs of the Bushveld Complex. Although large variations occur in thickness and composition, the Merensky Reef is generally < 30 cm thick and comprises a pegmatoidal feldspathic pyroxenite, bound above and below by thin (1-2 cm) chromitite seams (Fig. 3b). It is generally underlain by anorthosite and overlain by pyroxenite. Like the UG2 chromitite, the Merensky package locally cuts down into its footwall rocks to form potholes (Latypov et al. 2015).

Other examples of chromitite seams are found in the ~60 Ma Rum Layered Suite (NW Scotland; Emeleus et al. 1996). The Rum Layered Suite comprises the Eastern and Western Layered Intrusions and the Central Intrusion (ELI, WLI and CI, respectively). The ELI comprises 16 coupled peridotite-troctolite ± gabbro ± anorthosite macro-rhythmic units, each of which is considered to be the result of differentiation of batch fractionation within the Rum magma chamber (Brown, 1956; Emeleus et al. 1996). Thin (0.5 mm – 2 cm) chromitite seams formed in two principal environments. Chromitite seams drape the contacts of several of these units – for example, between the anorthositic tops (underneath) and peridotitic bases (above) of Units 6/7, 7/8 and 11/12 (O'Driscoll et al. 2010). These boundary chromitite seams are continuous over lateral distances of 100s of metres, generally maintaining a uniform thickness of ~2 mm around topographic culminations, depressions and even overhangs in the footwall anorthosite (Fig. 3c). Locally, pockets of chromitite protrude down into the underlying anorthosite; these were termed 'cone-structures' by O'Driscoll et al. (2010) and may represent small-scale analogues of the Bushveld potholes. The second mode of occurrence on Rum is as chromitite seams wholly contained within ELI and WLI peridotite bodies. These seams are more numerous than the boundary chromitites – hundreds have been documented from the Unit 10 peridotite alone, and there are likely to be thousands present in the ~420 m thick WLI (Hepworth et

al. 2017; 2018). These seams are also typically associated with a change in olivine texture on either side of them (Fig. 3d).

Many of the processes invoked for massive chromitites (e.g., magma mixing, crustal contamination) are also candidates for the formation of chromitite seams. Because the amount of Cr hosted in seams is so much less than massive layers, the mass balance problem is less acute. The complex field relations of the Merensky Reef chromitites, in particular around potholes (e.g., Latypov et al. 2015; 2017a), demonstrate that chromitites drape all parts of the outer edges of potholes, including vertical sidewalls and overhangs. These relations are very difficult to explain by crystal settling (or any sort of mechanical accumulation of chromite crystals) alone. Instead, they suggest that the chromitite crystallised in situ. Latypov et al. (2017b) emphasised magmatic erosion of the footwall to explain potholes and associated features, such as 'undercutting' MR, where sill-like bodies of chromitite from pothole edges protrude laterally into the footwall rocks.

Alternatively, it has been argued that chromitite seams may represent reaction products rather than products of direct crystallisation. For example, Nicholson and Mathez (1991) proposed that the Merensky Reef chromitites formed at metasomatic fronts, driven by dissolution of the crystal mush by percolating H_2O-rich melts. The presence of H_2O during these reactions causes the crystallisation temperatures of all of the coexisting silicate phases (relative to chromite) to be suppressed, allowing the latter to crystallise alone. This suggestion has similarities to the hydration melting model of Boudreau (2016) for the Stillwater massive chromitites. Mathez and Kinzler (2017) drew attention to the similarities between the Merensky and Rum chromitite seams. The Rum unit boundary seams were initially interpreted in the context of the batch fractionation model for the ELI macro-rhythmic units; so that a new replenishment of magma would first crystallise chromite which, after gravitational settling to form a chromitite seam, would be followed by successive crystallisation and settling of olivine and olivine + plagioclase to form the overlying peridotite and troctolite portions of each unit

(cf. Brown, 1956). However, the observation that the Rum chromitites faithfully follow footwall topography, including overhangs, without significant changes in seam thickness, led to a reevaluation of the traditional crystal settling model for chromitite formation and a proposal that new batches of superheated magma might thermochemically erode their footwall on entry to the magma chamber (O'Driscoll et al. 2010). In the latter scenario, chromitites represent an in situ reaction product between the underlying feldspathic cumulate and the incoming primitive magma, where assimilated troctolitic cumulate modified the composition of the magma to the extent that it crystallised chromite alone. Subsequent studies have interpreted the intra-peridotite chromitite seams in a similar way, such that reactive infiltration within the crystal mush occurred as a consequence of the incoming magma being emplaced into the crystal mush rather than onto the magma chamber floor (Hepworth et al. 2017; 2018).

4. Magnetite-Ilmenite Ti-V

Layered mafic-ultramafic intrusions become enriched in titanium (Ti) and vanadium (V) in their more fractionated portions and economic Fe-Ti-V resources may consequently form. The dominant minerals are ilmenite (as part of the ilmenite-haematite solid solution series) and titanomagnetite (as part of the ulvöspinel-magnetite solid solution series) – Figure 5. Titanium is a major component in both ilmenite ($FeTiO_3$) and the ulvöspinel component of titanomagnetite (Fe_2TiO_4 – Fe_3O_4). In contrast, vanadium partitions into titanomagnetite and to a lesser extent ilmenite where it substitutes for Fe^{3+} (Fig. 5). Notable resources include the Bushveld Complex in South Africa, the Panzhihua Intrusion in China, Windimurra Igneous Complex in Australia, and the Mustavaara Fe-Ti-V oxide deposit in Finland (Figure 2 and see Table 1). Resources within LMI are typically stratiform layers that accumulated at the bases of the magma chambers. Additional resources are found in norite dykes and intrusions associated with anorthosite provinces – notably at Allard Lake in Canada and Tellnes in Norway.

4.1 Source regions

Similar to other metals discussed in this chapter, titanium and vanadium enter mafic-ultramafic magma during partial melting of the mantle. While mid-ocean ridge basalt is low in Ti (1.53 wt.% TiO_2) and V (280 ppm) (Gale et al. 2013), many mantle hot spots produce lavas with much higher concentrations (for example, up to 5 wt.% TiO_2 and 500 ppm V in the Scoresby Sund basalts of Greenland (Larsen et al. 1989) and up to 4.3 wt.% TiO_2 and 405 ppm V (Peate 1997) in the Paraná basalts of Brazil). These concentrations reflect variations in the mantle source, notably the abundance of the dominant Ti and V hosts (phlogopite, rutile and perovskite; Foley et al. 2000; Corgne and Wood 2002). The elevated concentrations are indicative of contributions from mantle material that either hasn't been depleted by melt extraction, or become enriched through subduction, melt or volatile addition (from subcontinental lithospheric mantle). Mafic-ultramafic magmas derived from hot spots (and thus LMI) are, therefore, much more fertile for Ti and V than their mid-ocean ridge equivalents.

4.2 Titanomagnetite and ilmenite crystallisation

As mafic-ultramafic magmas start to crystallize, Ti and V become concentrated into the residual melt fraction. Ultramafic cumulates do not contain much Ti or V, and the crystallization of chromite ceases before ilmenite and titanomagnetite start to form. There is typically a significant stratigraphic separation (known as the spinel gap) in many LMI between the deepest strata that carry chromite (at the base of the magmatic stratigraphy) and the upper layers that carry ilmenite and titanomagnetite.

Ilmenite and titanomagnetite crystallisation is controlled by the availability of Ti, Fe, Si and O in the magma. The minerals crystallize as separate, homogeneous grains of (haematite-bearing) ilmenite and ulvöspinel-rich titanomagnetite. The partitioning of Fe and Ti is governed by the equilibrium

$$Fe_2TiO_4+Fe_2O_3 \leftrightarrow FeTiO_3+Fe_3O_4,$$

which is sensitive to temperature and the oxidation state of iron (Fe^{2+} and Fe^{3+}, which reflects the prevailing oxygen fugacity) (Fig. 5). This equilibrium is commonly used as a geothermometer and oxygen barometer. In mafic-ultramafic magmatic systems, the element partitioning is part of the

289 wider equilibrium that also encompasses iron-bearing mafic silicates and quartz (Lindsley et al. 1990;
290 Andersen et al. 1993; Sauerzapf et al. 2008). During primary crystallization, ilmenite carries significant
291 haematite in solution and titanomagnetite is ulvöspinel-rich. Therefore, the primary magmatic
292 assemblage may cause significant Ti to be partitioned into titanomagnetite (Fig. 5).

293 Vanadium is highly compatible in the titanomagnetite crystal lattice. Consequently, once
294 titanomagnetite starts to crystallize, the residual magma becomes rapidly depleted in V (Fig. 6a). As
295 dense minerals accumulate on the floor of a magma chamber, the lowermost, first-formed magnetite-
296 rich layer will therefore contain the highest V content (Fig. 6b).

297 ***4.3 Late- or post-magmatic evolution***

298 During cooling, titanomagnetite is prone to oxidation leading to a transformation known as "oxy-
299 exsolution" (Lindsley, 1991; Fig. 5). This process converts ulvöspinel to ilmenite and magnetite,
300 following the reaction:

301 $$6Fe_2TiO_4+O_2 \leftrightarrow 6FeTiO_3+2Fe_3O_4$$

302 Ilmenite cannot remain in solid solution and segregates to form lamellae, subgrains or trellis-
303 microstructures within the titanomagnetite host. The composition of the exsolved ilmenite and
304 remaining titanomagnetite reflects the temperature and oxygen fugacity at the time of exsolution (Fig.
305 5). The lower the temperature, the purer the ilmenite and magnetite. Conversely, the size of these
306 exsolved sub-grains is controlled by the diffusion of Fe and Ti, and diffusion rates are generally highest
307 at high temperature. Titanomagnetite-ilmenite intergrowths are ubiquitous within mafic igneous
308 rocks (Fig. 5). The scale and purity of the mineral pairs strongly influence the potential for mineral
309 processing and therefore the economic prospects of metal recovery. An ideal ore will have undergone
310 prolonged oxy-exsolution to low temperature at a slow enough rate for the exsolved minerals to
311 separate into large grains.

312 ***4.4 Formation of economic resources***

While the mineral chemistry of ilmenite and titanomagnetite is well understood, the process of ore formation in LMI is still enigmatic. The traditional view is that the minerals crystallize from their host magmas and settle (because of their high specific gravity) to the base of the magma chamber. However, Ti and V have similar mass balance problems as Cr, mentioned above. Mafic magmas reach saturation with ilmenite and titanomagnetite at TiO_2 contents of less than 5 wt.%, so there remains a problem as to how rocks with >60 wt.% of these minerals (such as the Main Magnetite Layer in the Bushveld complex, Cawthorn and Ashwal 2009) can form. Unlike chromite, phase relations do not support crystallization of ilmenite and/or titanomagnetite without simultaneous crystallization of pyroxene and plagioclase. It is therefore not feasible that such concentrations can be achieved by crystal accumulation alone since this would require an extremely efficient sorting mechanism. This problem is linked to the question as to whether residual magmas become iron- or silica-enriched during progressive fractionation (e.g., Hunter and Sparks 1987; Brooks et al. 1991; Tegner 1997).

The issues outlined above have led to the realization that many mafic magmas separate into conjugate, or immiscible, Si-rich and Fe-rich magmas as they fractionate (McBirney 1975; Charlier et al. 2011; Holness et al. 2011; Namur et al. 2012). The Fe-rich magmas may contain up to 40 wt.% FeO and 3 wt.% TiO_2, as well as up to 18 wt.% P_2O_5 (Hou et al. 2018). These magmas are dense and likely to become preferentially incorporated into the cumulates at the bottom of LMI – by contrast, the Si-rich magmas are relatively buoyant and may eventually percolate into the roof zone (Nielsen et al. 2015). Erosion of layered intrusions preferentially removes the Si-rich upper parts, leading to over-representation of their deeper Fe-rich portions. The immiscibility of Fe-rich magma offers an additional mechanism of fractionation and provides a feasible explanation for the concentration of ilmenite and titanomagnetite in LMI. Interestingly, it also offers a linkage between the evolution of LMI and a group of enigmatic magnetite-apatite ores known as Nelsonites or Kiruna-type iron ores (e.g., Nyström and Henríquez 1994; Tornos et al. 2016).

5. PGE-Ni-(Co-Cu-Au) mineralisation

Like other magmatic ore deposits mentioned in this chapter, mineralisation of precious metal magmatic sulphide deposits can be considered in terms of a source, a pathway, and mechanisms for collection of the metals of interest (Fig. 1). Magmatic sulphide deposits are accumulations of immiscible sulphide melt which segregated from a silicate magma and within which elevated concentrations of base and precious metals occur. Magmatic sulphide deposits are intrinsically polymetallic but can be categorised into (i) precious metal PGE-Ni-(Co-Cu-Au) and (ii) base metal Ni-Cu-(Co-PGE) deposits (where those elements listed in brackets are by-products). Precious metal magmatic sulphide deposits typically form stratiform ore bodies (or 'reefs') in LMI and generally comprise a low volume (< 1 modal %) of sulphide minerals. In this section, we will outline the factors that control the formation of PGE and nickel (Ni) magmatic sulphides, with their concentrations of less abundant cobalt (Co), copper (Cu) and gold (Au).

5.1 Source regions

The processes governing mineralisation of the PGE (Os, Ir, Ru, Rh, Pt, Pd), Ni, and to some extent Co, Cu and Au, are interlinked due to their affinity for sulphide melts at mantle and crustal conditions – hence their geochemical behaviour is broadly classified as chalcophile. The PGE have traditionally been further subdivided into a compatible Ir-group (IPGE) and an incompatible Pt-group PGE (PPGE), based on their behaviour during partial melting of the mantle (Table 1). The IPGE (Os, Ir and Ru, which behave in a similar fashion to Ni and Co) are sometimes hosted as nano- or microscale platinum-group minerals (Pitcher et al., 2009) within silicate and oxide minerals, especially olivine and spinel (chromite)). In contrast, the PPGE (Rh, Pt and Pd, with similar behaviour to Au and Cu) are incompatible with silicate and oxide minerals and largely hosted by sulphides in the mantle (Lorand and Luguet, 2016).

As partial melting starts, the most easily fusible minerals in the mantle source region will melt first – typically clinopyroxene, garnet and sulphides – and continued melting incorporates increasing amounts of spinel and olivine (Pearson, 2005and Figure 7). Progressively higher degrees of partial melting (expressed as melt fraction, F) incorporate more sulphides, until the sulphide budget of the source is exhausted. Given the strong affinity of chalcophile elements, and in particular the PPGE, for sulphide (expressed as high partition coefficients, D_i), any residual sulphide in the mantle source will suppress the uptake of PGE into the melt being formed. Thus, silicate magmas which are S-saturated are not fertile for PGE. In contrast, if melting continues to the point of sulphide exhaustion, the full PGE budget of the mantle source will be imparted to the S-undersaturated silicate magma, maximising magma fertility for the PGE (Fig. 7). Beyond this point, continued melting merely dilutes the concentration of these elements in the silicate magma. For example, assuming a peridotite mantle source with a starting concentration of 200 ppm S, all sulphides would be melted and dissolved in a silicate magma by the time F=13.5% of equilibrium batch partial melting (Naldrett, 2011). In this model, fractionation of the PGE in the mantle occurs largely because of the different melting points of the minerals hosting these elements (i.e., sulphide *vs* oxide – Fig. 7). Ore deposit formation models are based upon this paradigm and can be used to describe the fertility of basaltic magmatic systems for PGE-Ni-(Co-Cu-Au) mineralisation.

Whilst this paradigm is broadly applicable, empirical studies of mantle sulphides have shown that other factors influence the behaviour of the PGE, Ni, Co, Cu and Au during partial melting. For most pressures and temperatures at which partial melting takes place, the mantle sulphide budget occurs as two coexisting sulphide phases (e.g., Bockrath et al., 2004; Lorand and Luguet, 2016) – a crystalline Fe-rich monosulphide solid solution (MSS) relatively enriched in IPGE, and an immiscible molten Ni-Cu sulphide enriched in PPGE (Fig. 8). During partial melting, the immiscible sulphide gradually becomes incorporated into silicate magma, while the MSS tends to be retained in the mantle source. Thus, silicate magmas derived from mantle partial melting are generally enriched in PPGE and depleted in IPGE, relative to the initial bulk mantle composition (Bockrath et al., 2004).

Empirical studies have also shown that the sulphides in different mantle lithologies (e.g., peridotite *vs.* eclogite; McDonald et al., 2017) and reservoirs (i.e., enriched or depleted; Hamlyn and Keays, 1986) may have very different metal budgets. Furthermore, multiple generations of sulphides may be present within a single mantle reservoir, with each generation preserving a distinct precious metal inventory (Hughes et al., 2017). Some mantle sulphides are interstitial to the major silicate and oxide minerals within that reservoir, but other sulphides may occur as inclusions within these minerals. Thus, mantle sulphides may not always be available for entrainment into silicate magmas during partial melting and, if entrained, will impart varying precious metal characteristics to that silicate magma. Yet classic models (e.g., Fig. 7) used to predict the fertility of mantle-derived magmas assume that interstitial sulphides of uniform composition are always accessible for melting. Unravelling these discrepancies leads to a better understanding of why certain parts of the Earth's crust appear pre-disposed to precious metal mineralisation.

5.2 Mechanisms of mineralisation

Fertile, S-unsaturated silicate magma ascends from a partially melted mantle source reservoir through the lithosphere. The decrease in pressure associated with this ascent increases the ability of the silicate magma to dissolve S such that the Sulphur Content at Sulphide Saturation (SCSS) increases (Li and Ripley, 2005). This inverse relationship between pressure and SCSS means that without further modification the magma would be unlikely to reach S-saturation leading to mineralisation. The following subsections outline mechanisms by which a silicate magma may reach S-saturation in the crust, in order to form an immiscible sulphide liquid that can accumulate to form an ore deposit.

An important consideration in the mineralisation of PGE-Ni-(Co-Cu-Au) deposits is the volume of sulphide in the magmatic system. This is described as the mass ratio of the silicate magma divided by that of the sulphide liquid, termed the R-factor (Campbell and Naldrett, 1979):

413 $$R = \frac{m_{silicate}}{m_{sulphide}}$$

412

414 Given the very high partition coefficients of the PGE from silicate magma into sulphide (several orders
415 of magnitude greater than D_{Ni} or D_{Cu}), the optimal concentrations of PGE in sulphide (the tenor) will
416 be achieved in smaller volumes of sulphide. Therefore, deposits with a high R-factor (e.g., > 10^4) have
417 low volumes of high tenor sulphide (Fig. 9). However, the efficiency with which an immiscible sulphide
418 liquid circulates in a silicate magma, and therefore the extent to which chalcophile metals diffuse into
419 the sulphide liquid, is also a function of the R-factor (Mungall, 2002) – Figure 9.

420 The formation of a potentially economic ore deposit requires the accumulation of this small volume
421 of sulphide liquid into a narrow stratiform horizon (or reef), again usually at the base of the magma
422 chamber. In some cases, sulphide abundance may be so low that mineralisation is not easily visible.
423 Thus, an understanding of the mechanisms of mineralisation in LMI facilitates exploration for new
424 PGE-Ni-(Co-Cu-Au) reefs.

425 ***Magma mixing:*** Replenishment of a silicate magma chamber with a new pulse of magma can lead to
426 S-oversaturation. This appears to be particularly effective in magmatic systems with a significant
427 ultramafic component, and for magmas close to S-saturation prior to mixing. During magma mixing,
428 several factors can contribute to a magmatic system achieving S-saturation. These are (i) pressure
429 changes associated with the introduction of a new magma batch (increasing pressure leads to a
430 decrease in SCSS), (ii) temperature changes (increasing temperature causes an increase in SCSS) and
431 (iii) compositional changes such that increasing FeO content results in an increase in SCSS (Wykes et
432 al., 2014). These factors are summarised in Figure 10, which shows how magma mixing may lead to S-
433 saturation in compositional space.

434 As with the formation of chromitite layers, open-system replenishments are thought to underpin the
435 formation of many classic PGE-Ni-(Co-Cu-Au) reefs. Most notable amongst these are the Merensky

436 Reef and UG-2 of the Bushveld Complex in South Africa. Other examples include the Main Sulphide
437 Zone of the Great Dyke in Zimbabwe,the Munni Munni Complex in Australia, Penikat and Portimo (and
438 other Fennoscandian intrusions) and other smaller bodies such as the Rum Layered Suite.

439 ***Fractional crystallisation:*** During fractional crystallisation of a basaltic silicate magma, the compatible
440 chalcophile elements (Ni, Co, IPGE) gradually become incorporated (by partitioning or as discrete
441 PGM) into minerals such as olivine and chromite. This fractionation may be monitored, for example,
442 by the abundance of Ni in olivine – early-formed olivine (i.e., with high forsterite content) will contain
443 higher abundances of Ni than low-Fo olivine formed much later in the fractionating assemblage. In
444 contrast, incompatible chalcophlile elements (PPGE, Cu, Au) and S will not be incorporated into silicate
445 and oxide mineral phases during fractional crystallisation and consequently the concentration of these
446 elements increases in the residual silicate magma. The increase in S concentration, coupled with
447 cooling, can culminate in the silicate magma reaching S-saturation (Fig. 10), with the accompanying
448 segregation of a fraction of immiscible sulphide liquid into which all remaining chalcophile elements
449 partition (Table 1). Thus, prolonged fractional crystallisation (typically > 40% crystallisation; Naldrett,
450 2011) can achieve S-saturation with a high R-factor.

451 Protracted fractionation has implications for the relative proportions of chalcophile elements in a
452 potentially mineralised sulphide-bearing layer, as well as for the location of the resultant reef in the
453 LMI. For example, mineralisation may be particularly enriched in PPGE (especially Pd), Cu and Au, but
454 have extremely low abundances of IPGE and Ni in comparison to other reefs formed via different
455 mechanisms (such as magma mixing). These Pd-Au-Cu enriched reefs may also occur higher in the
456 layered sequence and be associated with gabbroic cumulates, as opposed to pyroxenitic or noritic
457 cumulates lower down in the magmatic succession. Notable examples of reefs formed by extended
458 fractional crystallisation include the Platinova Reef of the Skaergaard Intrusion in Greenland, Sonju
459 Lake and the Layered Series at Duluth in the USA. These magmatic systems may not have incorporated
460 any new magma injections and the Skaergaard Intrusion is a notable case where protracted magmatic

differentiation resulted in the formation of the Platinova Reef relatively high up in the layered sequence (Nielsen et al., 2015).

***Contamination**:* Contamination of a basaltic magma by addition of silica (by assimilation of silica-rich sedimentary sequences or silica-rich melts from wall rock anataxis) or carbon-rich crustal lithologies (such as mudrocks, graphite, coal, etc) may trigger a redox-controlled S-saturation event (Fig. 10). Most effective, however, is the contamination of basaltic magmas with sulphide-rich crustal rocks (such as shales, evaporates and coal) mainly because this increases the concentration of S in the magma, inducing S-oversaturation (Ripley and Li, 2013). This process generally leads to the production of large volumes of sulphide liquid and thus a magmatic system with low R-factor. Sulphides produced in this way tend to have much lower concentrations of PGE than sulphides in high R-factor magmatic systems. As a result, the mechanism of crustal contamination could be considered, in certain cases, to be counterproductive to the formation of stratiform PGE-Ni-(Co-Cu-Au) reefs in LMI.

In other cases, however, evidence from stable isotopes ($\delta^{34}S$ or $\Delta^{33}S$) indicates that contamination may in fact have played an important role, particularly during the formation of several well-known examples of PGE-Ni-(Co-Cu-Au) mineralisation such as the Platreef in the Northern Limb of the Bushveld Complex (Kinnaird and McDonald, 2018) and the Ahmavaara deposit of the Suhanko Intrusion in Finland (Makkonen et al., 2017). The impact of contamination on the formation of PGM mineralisation associated with high tenor sulphides is still debated, particularly in the case of the Platreef (Kinnaird and McDonald, 2018). Studies indicate that the high tenor Platreef sulphides may have formed deeper in the magmatic plumbing system and prior to local contamination of the Platreef parental magma. The high tenor sulphide liquid was then transported via the magma conduits to the current level of the Platreef and was ultimately responsible for the mineralisation seen today. If this is correct then the widespread local contamination of the Platreef footwall by S-rich crustal rocks is not likely to have been an important ore-forming process in this deposit.

***Fluids**:* Hydrothermal or deuteric high-temperature late-magmatic hydrous fluids may play an important role in the formation of PGE reefs. Models for fluid-based mineralisation in LMI generally suggest that the chalcophile elements and S are scavenged by upward-migrating fluids percolating through the cooling cumulate pile. These fluids are exsolved from cooling intercumulus melt, may be aqueous, saline and carbonic in composition, are likely halogen-rich, and are capable of dissolving appreciable amounts of S and precious metals (e.g., Hanley et al., 2005). Notable examples of PGE-Ni-(Co-Cu-Au) mineralisation that have been attributed to metasomatic processes are the J-M Reef of the Stillwater Complex in Montana, USA (Boudreau, 1999) and the Merensky Reef in the Bushveld Complex (e.g., Ballhaus and Stumpfl, 1986; Kanitpanyacharoen and Boudreau, 2013). Recent studies have also highlighted the critical role of fluids in mineralisation in some portions of the Main Zone of the Bushveld Complex which were previously thought unmineralised, thus representing an exciting new exploration frontier (McFall et al., 2019).

6. The Future of LMI Resources

The transformation of society away from carbon-based fossil fuel will fundamentally change the resource industry. There will be a much greater demand for metals and minerals that are used in clean energy production, energy storage, and decarbonisation. LMI host important resources of Sc, PGE, Co, V and Mg-silicate minerals that will be essential for this transformation. Although not discussed in this article, the Mesoproterozoic Ilímaussaq layered intrusion of southern Greenland is highly enriched in the critical rare earth element (REE) metals and will undoubtedly play an important role in the availability of these metals to society in future decades.

6.1 Future uses and demands on existing commodities

Chromium has a well developed market for primary production and recycling. Stainless steel is not expected to undergo substantial market transforations in the cicrular economy, although there may be more emphasis on sustainable manufacturing and recycling.

Platinum-Group Elements (PGE) (particularly the PPGE) are extensively used in catalytic fuel emission converters (2-4 g used per catalytic converter) and as industrial catalysts. As society is expected to transition away from the use of fossil fuel, one might expect a long term decline in their demand. However, Pt and Pd are also important components in hydrogen fuel cells, where they are employed to catalyse the oxidation of hydrogen (currently requiring over 28 g of Pt per fuel cell). Fuel cell technology is attractive for mobile energy supply where batteries are not a viable option. While the automotive industry may develop into a large market, fuel cells are particularly attractive for the aviation industry, because of the much higher energy density of hydrogen (around 130 MJ/kg) than traditional aviation fuel (45 MJ/kg) and Li-ion batteries (0.5 MJ/kg).

Cobalt and nickel are important components of cathodes in lithium-ion batteries, and the metals are therefore critical for the development of energy storage systems. Lithium-ion batteries dominate the market for electric vehicles and domestic storage, and the demand is projected to surge with the transformation of the global vehicle fleet to electricity.

Copper is essential for electricity infrastructure. National and international power grids will need substantial expansion to deal with the demands from electrification of domestic vehicles as well as the wider transport sector. Further demands can be expected to reduce emissions from the industry sector.

Vanadium is used for energy storage in Vanadium Redox Batteries. An increased reliance on renewable energy sources (wind, solar) to replace coal- and oil-fuelled power stations requires storage solutions to secure continuous electricity supply. Their large capacity and ability to survive prolonged periods under complete discharge makes these batteries ideal for grid storage.

6.2 Future commodities

Scandium (Sc) partitions into clinopyroxene and hornblende and is locally concentrated into economically interesting resources in lateritic soils above zoned ultramafic complexes, such as Owendale and Nyngan in Australia. Given the mineralogical similarities, LMI (particularly those with alkaline affinities) may also host future scandium resources. Scandium alloyed with aluminium (Al) is a light and strong high-performance material that can be used to reduce the weight (and therefore the energy consumption) of airplanes and vehicles. Scandium is also used in solid oxide fuel cells.

Mg silicates (olivine, talc and serpentine) are essential for carbon capture technologies that offer permanent greenhouse gas removal. The reaction of atmospheric CO_2 with Mg silicate is energy positive, so although the slow reaction kinetics are problematic, the process is both energy efficient and energy economic. Other geological alternatives for carbon capture, such as underground storage in oil wells, cannot rival carbonation of magnesium silicate minerals in terms of capacity or permanency. Biological storage in the Earth's ecosystems is less efficient and far less permanent and would require extensive reforms of global land use. Considering that global carbon emissions exceed 10 billion tonnes per year (Boden et al, 2017), reductions in emission targets will invariably require large-scale development of cabon capture.

548

549 **Table captions**

550 **Table 1** – Summary of partitioning behaviour of metals discussed in this chapter, the grades and the
551 concentrations of metals in ore deposits relative to mantle abundances, key minerals in ore deposits,
552 uses and products of the relevant metals, and a selection of notable ore deposits worldwide. Note
553 that D_i* is the bulk partition coefficient between mantle minerals and silicate melt during partial
554 melting of the mantle, under conditions typical for the generation of basaltic magmas. D_i is the
555 partition coefficient for the typical phase which concentrates these elements (e.g., sulphide melt for
556 chalcophile elements like Cu and the PGE; oxides for Cr, V and Ti). The PPGE are the Pd-group
557 platinum-group elements (Rh, Pt, Pd) and IPGE are the Ir-group platinum-group elements (Os, Ir, Ru).
558 PGM in this table denotes the platinum-group minerals. Where elements are listed in brackets, this
559 indicates that these occur as co- or by-products of the main ores listed in this chapter. Information for
560 elements in brackets therefore does not show the main ore locations. Note that 1 ppm = 1 g/t.

561

562 **Figure captions**

563 **Figure 1** – Factors and processes governing mineralisation and the formation of an ore deposit.

564 **Figure 2** – (a) Chromitite: UG-1 chromitite seams (the dark bands) at Dwars River in the Bushveld
565 Complex. These chromitites bifurcate, may have irregular anastomosing contacts with underlying
566 anorthosites, and sometimes contain xenoliths of anorthosite. (b) PGE reef: Merensky Reef
567 photographed in an underground mine in the Western Bushveld. From bottom to top: anorthosite
568 footwall underlying the basal chromitite of the Merensky Reef package, the Merensky pegmatoid and
569 overlying feldspathic pyroxenite. In this image there are three chromitite stringers, including the basal
570 chromitite. (c) Magnetitite: Dark layers anomalously rich in ilmenite and titanomagnetite in the
571 Skaergaard intrusion, Greenland. Layering in the normal gabbro (observed toward the right) is much

poorer in these minerals. The layers are approximately planar and would have formed parallel to the magma chamber floor, the succession was rotated 20º after crystallisation. The undulating appearance is due to topography. The younging direction is to the right. Hammer for scale. (d) Magnetitite: Two metre thick dark titanomagnetite-rich layer in the Bushveld Complex, South Africa. Similar to Skaergaard, the layer would have formed along a planar surface parallel to the magma chamber floor. The younging direction is up. Photo courtesy of Paul Nex, University of the Witwatersrand.

Figure 3 – (a) Field photograph of the massive G chromitite of the Stillwater Complex, USA. Chromite is black and olivine is brown. Note the interlayering defined by the relative abundances of these two minerals. The entire chromitite package, as well as others in the Stillwater intrusion, is characterised by complex variations in chromite and olivine modal abundances and textural relationships. The person's finger on the left gives scale. (b) QEMSCAN® image showing the lower chromitite of the Merensky Reef package of the Bushveld Complex. The brownish-coloured crystals are orthopyroxene, blue is plagioclase, and black is chromite. Other (brightly-coloured) phases are accessory hydrous minerals (biotite, amphibole etc). (c) Field photograph of a chromitite seam (black) at the contact between peridotite (brown, above) and anorthosite (white, below) from the Unit 11-12 boundary of the ELS in the Rum Layered Suite. This is an oblique view showing the undulose character of the chromitite seam in cross section. The hand lens at the top of the photograph gives scale. (d) QEMSCAN® image of an intra-peridotite chromitite seam from Unit 10 (ELS, Rum Layered Suite). Way up is to the top left of the image. Olivine crystals are yellow, plagioclase is light blue and chromite is black. Other (secondary) phases such as serpentine and amphibole are represented by the dark blue, pink and purple colours. Note the change in texture (olivine grainsize reduction) across the chromitite seam.

Figure 4 – Ternary phase diagrams of the chromite-olivine-SiO_2 system illustrating possible models for chromitite formation in LMI. In (a), theoretical magma mixing and contamination are shown. A

possible 'normal' differentiation path (in orange) for a magma with starting composition is labelled A. Crystallisation of olivine will result in the liquid reaching the olivine-chromite cotectic, and eventually orthopyroxene saturation at the end of the orange path (after Irvine, 1977). Replenishment of the magma chamber and mixing of the primitive (B) and differentiated liquids (C, green dot) will move the hybrid composition into the chromite field and lead to crystallisation of chromite only (red dot). Contamination of the differentiating liquid by a SiO_2-rich assimilant (e.g., Spandler et al. 2005) also has the effect of moving the hybrid into the chromite-only field (blue dot/path). In (b), the effects of magma hydration are shown and, in particular, the expansion of the chromite phase field with addition of H_2O. The relatively dry liquid represented by the purple dot on the red dashed line is saturated in chromite and orthopyroxene. With H_2O addition, the phase boundaries shift (blue lines) and the liquid is saturated in chromite alone. See text for further discussion. Redrawn after Boudreau (2016) and references therein.

Figure 5 – Phase diagrams demonstrating exsolution of magnetite, ilmenite and spinel-group minerals with decreasing temperature, and the process of oxy-exsolution. (a) Crystallisation and cooling of Fe-Ti oxide minerals controlling distribution of V and Ti in ore (from Lindsley, 1991). (b) Stages in oxy-exsolution: (i) Oxidation of FeO to Fe_2O_3, (ii) Exsolution of equilibrium pair of titanomagnetite and ilmenite and (iii) Magnetite with ilmenite domains, lamellae-, or trellis-like textures.

Figure 6 – (a) Concentration of V in a fractionating magma crystallising magnetite. (b) Variations of magnetitite compositions in the Bushveld Upper Zone, based on Klemm et al. (1985).

Figure 7 – Partial melting of the mantle. (a) Cartoon demonstrating the partial melting process. Fusible mineral phases, including sulphides, melt first. In a partial melting model there will come a point that interstitial sulphides will become exhausted in the mantle source. (b) Sketch model of the concentration of key elements in the silicate magma formed through partial melting of the mantle. As sulphides host most of the chalcophile elements, they control the budget of these elements in the melts that are formed. Continued melting beyond the exhaustion of these sulphides effectively dilutes

622 the concentration of chalcophile elements in the melt, thus a theoretical peak fertility is defined. This
623 model is complicated by sulphides that may be included within other minerals and variation in the
624 trace element composition of mantle sulphides.

625 **Figure 8** – The physical state of mantle sulphides at a range of pressures and temperatures. The shaded
626 area delineates pressure and temperature conditions at which most mantle partial melting takes
627 place. Diagram adapted from Bockrath et al. (2004).

628 **Figure 9** – R-factor models for chalcophile elements Ni, Cu and Pt (as an example for the PGE): (a) The
629 concentration of elements according to various R-factor values for a silicate magmatic system with an
630 immiscible sulphide liquid, adapted from Campbell & Naldrett (1979) and assuming a starting
631 concentration of 250 ppm Ni, 70 ppm Cu and 10.5 ppb Pt. (b) Cartoon models visualising low and high
632 R-factor processes.

633 **Figure 10** – Processes that cause silicate-sulphide liquid immiscibility: Magma mixing, contamination
634 and incompatible concentration during fractional crystallisation change the mass fraction of Fe
635 (described as FeO) and S in the resultant magma, causing that magma to change from S-
636 undersaturated to S-saturated conditions. Diagram after Poulson & Ohmoto (1990).

637

638 **Suggested Further Reading**

639 Naldrett, A.J., 2011. Fundamentals of magmatic sulfide deposits. Rev. Econ. Geol. 17, 1–50.

640

641

642 **References**

643 Andersen, D.J., Lindsley, D.H., Davidson, P.M. 1993. QUILF: a pascal program to access equilibria
644 among Fe-Mg-Mn-Ti oxides, pyroxenes, olivine and quartz. Computers and Geosciences. 19,

1333-1350.

Ballhaus, C.G., Stumpfl, E.F. 1986. Sulfide and platinum mineralization in the Merensky Reef: evidence from hydrous silicates and fluid inclusions. Contrib. to Mineral. Petrol. 94, 193–204. https://doi.org/10.1007/BF00592936.

Bockrath, C., Ballhaus, C., Holzheid, A. 2004. Fractionation of the Platinum-Group Elements During Mantle Melting. Science. 305(80), 1951–1953. https://doi.org/10.1126/science.1100160.

Boden, T.A., Marland, G., and Andres, R.J. 2017. Global, Regional, and National Fossil-Fuel CO_2 Emissions. Carbon Dioxide Information Analysis Center, Oak Ridge National Laboratory, U.S. Department of Energy, Oak Ridge, Tenn., U.S.A. doi 10.3334/CDIAC/00001_V2017.

Boudreau, A. 1999. Fluid fluxing of cumulates: The J-M reef and associated rocks of the stillwater complex, Montana. J. Petrol. 40, 755–772. https://doi.org/10.1093/petroj/40.5.755.

Boudreau, A.E. 2016. The Stillwater Complex, Montana – Overview and the significance of volatiles. Vol. 80(4), 585–637.

Brooks, C.K., Larsen, L.M., Nielsen, T.F.D. 1991. Importance of iron-rich tholeiitic magmas at divergent plate margins: A reappraisal. Geology. 19, 269-272.

Brown, G.M. 1956. The layered ultrabasic rocks of Rhum, Inner Hebrides. PhilosophicalTransactions of the Royal Society of London. Series B. 240, 1-53.

Campbell, I., Naldrett, A.J. 1979. The influence of silicate-sulphide ratios on the Geochemistry of Magmatic Sulphides. Econ. Geol. 74, 1503–1506. https://doi.org/10.2113/gsecongeo.74.6.1503.

Cawthorn, R. G. 2015 in Layered Intrusions. Eds. Charlier B., Namur, O., Latypov R. & Tegner, C. 517–587 (Springer, New York, NY).

Cawthorn, R.G., Ashwal, L.D. 2009. Origin of Anorthosite and Magnetitite Layers in the Bushveld Complex, Constrained by Major Element Compositions of Plagioclase. Journal of Petrology. 50, 1607-1637.

Charlier, B., Duchesne, J.C., Vander Auwera, J. 2006. Magma chamber processes in the Tellnes

671 ilmenite deposit (Rogaland Anorthosite Province, SW Norway) and the formation of Fe–Ti ores
672 in massif-type anorthosites. Chemical Geology. 234, 264-290.
673 Charlier, B., Namur, O., Toplis, M.J., Schiano, P., Cluzel, N., Higgins, M.D., Auwera, J.V. 2011. Large-
674 scale silicate liquid immiscibility during differentiation of tholeiitic basalt to granite and the
675 origin of the Daly gap. Geology. 39, 907-910.
676 Corgne, A., Wood, B.J. 2002. $CaSiO_3$ and $CaTiO_3$ perovskite-melt partitioning of trace elements:
677 Implications for gross mantle differentiation. Geophysical Research Letters. 29, 31-39.
678 Foley, S.F., Barth, M.G., Jenner, G.A. 2000. Rutile/melt partition coefficients for trace elements and
679 an assessment of the influence of rutile on the trace element characteristics of subduction
680 zone magmas. Geochimica et Cosmochimica Acta. 64, 933-938.
681 Gale, A., Dalton, C.A., Langmuir, C.H., Su, Y., Schilling, J-G. 2013. The mean composition of ocean
682 ridge basalts. Geochemistry, Geophysics, Geosystems. 14, 489-518.
683 Hamlyn, P.R., Keays, R.R. 1986. Sulfur saturation and second-stage melts: application to the Bushveld
684 platinum metal deposits. Econ. Geol. 81, 1431–1445.
685 https://doi.org/10.2113/gsecongeo.81.6.1431.
686 Hanley, J.J., Mungall, J.E., Pettke, T., Spooner, E.T.C., Bray, C.J. 2008. Fluid and Halide Melt Inclusions
687 of Magmatic Origin in the Ultramafic and Lower Banded Series, Stillwater Complex, Montana,
688 USA. J. Petrol. 49, 1133–1160. https://doi.org/10.1093/petrology/egn020.
689 Hanley, J.J., Pettke, T., Mungall, J.E., Spooner, E.T.C. 2005. The solubility of platinum and gold in NaCl
690 brines at 1.5 kbar, 600 to 800°C: A laser ablation ICP-MS pilot study of synthetic fluid
691 inclusions. Geochim. Cosmochim. Acta. 69, 2593-2611.
692 https://doi.org/10.1016/j.gca.2004.11.005.
693 Hepworth, L.N., O'Driscoll, B., Gertisser, R., Daly, J.S., Emeleus, C.H. 2017. Linking In Situ Crystallization
694 and Magma Replenishment via Sill Intrusion in the Rum Western Layered Intrusion, NW
695 Scotland. Journal of Petrology. 59(8), 1605–1642.

696 Hepworth, L.N., O'Driscoll, B., Gertisser, R., Daly, J.S., Emeleus, C.H. 2017. Incremental construction of
697 the Unit 10 peridotite, Rum Eastern Layered Intrusion, NW Scotland. Journal of Petrology. 58(1),
698 137-166.
699 Holness, M.B., Stripp, G., Humphreys, M.C.S., Veksler, I.V., Nielsen, T.F.D., Tegner, C. 2011. Silicate
700 Liquid Immiscibility within the Crystal Mush: Late-stage Magmatic Microstructures in the
701 Skaergaard Intrusion, East Greenland. Journal of Petrology. 52, 175-222.
702 Horan, M.F., Morgan, J.W.,Walker, R.J., Cooper, R.W. 2001. Re-Os isotopic constraints on magma
703 mixing in the Peridotite zone of the Stillwater Complex, Montana, USA. Contributions to
704 Mineralogy and Petrology. 141, 446–457.
705 Hou, T., Charlier, B., Holtz, F., Veksler, I., Zhang, Z., Thomas, R., Namur, O. 2018. Immiscible hydrous
706 Fe–Ca–P melt and the origin of iron oxide-apatite ore deposits. Nature Communications. 9,
707 1415-1423.
708 Hughes, H.S.R., McDonald, I., Loocke, M., Butler, I.B., Upton, B.G.J., Faithfull, J.W. 2017. Paradoxical
709 co-existing base metal sulphides in the mantle: The multi-event record preserved in Loch Roag
710 peridotite xenoliths, North Atlantic Craton. Lithos. 276, 103–121.
711 https://doi.org/10.1016/j.lithos.2016.09.035.
712 Hunter, R.H., Sparks, R.S.J. 1987. The Differentiation of the Skaergaard Intrusion. Contributions to
713 Mineralogy and Petrology 95: 451-461.
714 Irvine, T. N. 1977. Origin of chromitite layers in the Muskox intrusion and other stratiform intrusions:
715 a new interpretation. Geology. 5, 273–277.
716 Junge, M., Oberthür, T. & Melcher, F. 2014. Cryptic variation of chromite chemistry, platinum group
717 element and platinum group mineral distribution in the UG-2 chromitite: an example from the
718 Karee Mine, Western Bushveld Complex, South Africa. Econ. Geol. 109, 795–810.
719 Kanitpanyacharoen, W., Boudreau, A.E. 2013. Sulfide-associated mineral assemblages in the
720 Bushveld Complex, South Africa: Platinum-group element enrichment by vapor refining by
721 chloride-carbonate fluids. Miner. Depos. 48, 193–210. https://doi.org/10.1007/s00126-012-

722 0427-2.
723 Kinnaird, J.A., McDonald, I. 2018. The Northern Limb of the Bushveld Complex: A New Economic
724 Frontier. Met. Miner. Soc. https://doi.org/10.5382/SP.21.08.
725 Klemm, D.D., Henckel, J., Dehm, R.M. and Von Gruenewaldt, G. 1985. The geochemistry of
726 titanomagnetite in magnetite layers and their host rocks of the eastern Bushveld Complex.
727 Economic Geology. 80(4), 1075-1088.
728 Larsen, L.M., Watt, W.S., Watt, M. 1989. Geology and petrology of the Lower Tertiary plateau basalts
729 of the Scoresby Sund region, East Greenland. Bulletin of the Greenland Geological Survey 157,
730 164.
731 Latypov, R.M, O'Driscoll, B., Lavrenchuk, A. 2013. Towards a model for an in situ origin for PGE reefs
732 in layered intrusions: insights from the chromitite seams of the Rum Eastern Layered
733 Intrusion, Scotland. Contributions to Mineralogy and Petrology. 166(1), 309-327.
734 Latypov, R.M., Chistyakova, S., Yu, Page, A. & Hornsey, R. 2015. Field evidence for the in situ
735 crystallization of the Merensky Reef. J. Petrol. 56, 2341–2372.
736 Latypov, R.M., Chistyakova, S., Yu. & Mukherjee, R.A. 2017a. Novel hypothesis for origin of massive
737 chromitites in the Bushveld Igneous Complex. J. Petrol. 59(10), 1899-1940.
738 https://doi.org/10.1093/petrology/egx077.
739 Latypov, R.M., Chistyakova, S., Yu, Barnes, S.J. & Hunt, E.J. 2017b. Origin of platinum deposits in
740 layered intrusions by in situ crystallization: evidence from undercutting Merensky Reef of the
741 Bushveld Complex. J. Petrol. 58, 715–761.
742 Li, C., Ripley, E.M. 2005. Empirical equations to predict the sulfur content of mafic magmas at sulfide
743 saturation and applications to magmatic sulfide deposits. Miner. Depos. 40, 218–230.
744 https://doi.org/10.1007/s00126-005-0478-8.
745 Lindsley, D.H. 1991. Experimental Studies of Oxide Minerals. In: D. H. Lindsley. Oxide Minerals:
746 Petrographic and Magnetic Significance. Reviews in Mineralogy. 25, 69-106.
747 Lindsley, D.H., Frost, B.R., Andersen, D.J., Davidson, P.M. 1990. Fe-Ti oxide-silicate equilibria:

748 Assemblages with orthopyroxene. In: Spencer, R.J., I-M C (eds) Fluid-mineral interactions: A
749 tribute to H.P. Eugster. Geochemical Society Special Paper, 103-119.
750 Lipin, B.R. 1993. Pressure increases, the formation of chromite seams, and the development of the
751 ultramafic series in the Stillwater complex, Montana. J. Petrol. 34, 955–976.
752 Lorand, J.-P., Luguet, A. 2016. Chalcophile and siderophile elements in mantle rocks: Trace elements
753 controlled by trace minerals. Rev. Mineral. Geochemistry. 81, 441–488.
754 https://doi.org/10.2138/rmg.2016.81.08.
755 Makkonen, H.V., Halkoaho, T., Konnunaho, J., Rasilainen, K., Kontinen, A., Eilu, P. 2017. Ni-(Cu-PGE)
756 deposits in Finland – Geology and exploration potential. Ore Geol. Rev. 90, 667–696.
757 https://doi.org/10.1016/j.oregeorev.2017.06.008.
758 Mathez, E.A., Kinzler, R.J. 2017. Metasomatic chromitite seams in the Bushveld and Rum Intrusions.
759 Elements. 13, 397-402.
760 McBirney, A.R. 1975. Differentiation of the Skaergaard Intrusion. Nature. 253, 691-694.
761 McDonald, I., Vaughan, D.J. and Tredoux, M. 1995. Platinum mineralization in quartz veins near
762 Naboomspruit, central Transvaal. South African Journal of Geology. 98(2), 168-175.
763 McDonald, I., Hughes, H.S.R., Butler, I.B., Harris, J.W., Muir, D. 2017. Homogenisation of sulphide
764 inclusions within diamonds: A new approach to diamond inclusion geochemistry. Geochim.
765 Cosmochim. Acta. 216, 335–357. https://doi.org/10.1016/j.gca.2017.04.039.
766 McFall, K., McDonald, I., Tanner, D., Harmer, R.E. 2019. The mineralogy and mineral associations of
767 platinum-group elements and precious metals in the Aurora Cu-Ni-Au-PGE deposit, Northern
768 Limb, Bushveld Complex. Ore Geol. Rev. 106, 403–422.
769 https://doi.org/10.1016/j.oregeorev.2019.02.008.
770 Mondal, S.K. and Mathez, E.A. 2007. Origin of the UG2 chromitite layer, Bushveld Complex. J. Petrol.
771 48, 495–510.
772 Mungall, J.E. 2002. Kinetic Controls on the Partitioning of Trace Elements Between Silicate and
773 Sulfide Liquids. J. Petrol. 43, 749–768. https://doi.org/10.1093/petrology/43.5.749.

774 Mungall J.E., Naldrett A.J. 2008. Ore deposits of the platinum-group elements. Elements. 4, 253-258.
775 Naldrett, A.J. 2011. Fundamentals of magmatic sulfide deposits. Rev. Econ. Geol. 17, 1–50.
776 Namur, O., Charlier, B., Holness, M.B. 2012. Dual origin of Fe–Ti–P gabbros by immiscibility and
777 fractional crystallization of evolved tholeiitic basalts in the Sept Iles layered intrusion. Lithos.
778 154, 100-114.
779 Nicholson, D.M. and Mathez, E.A. 1991. Petrogenesis of the Merensky Reef in the Rustenburg section
780 of the Bushveld Complex. Contributions to Mineralogy and Petrology. 107, 293–309.
781 Nielsen, T.F.D., Andersen, J.C.Ø., Holness, M.B., Keiding, J.K., Rudashevsky, N.S., Rudashevsky, V.N.,
782 Salmonsen, L.P., Tegner, C., Veksler, I.V. 2015. The Skaergaard PGE and Gold Deposit: the
783 Result of in situ Fractionation, Sulphide Saturation, and Magma Chamber-scale Precious Metal
784 Redistribution by Immiscible Fe-rich Melt. Journal of Petrology. 56, 1643-1676.
785 Nyström J.O., Henríquez F. 1994. Magmatic Features of Iron Ores of the Kiruna Type in Chile and
786 Sweden: Ore Textures and Magnetite Geochemistry. Economic Geology. 89, 820-839.
787 O'Driscoll, B., Emeleus, C.H., Donaldson, C.H. & Daly, J.S. 2010. Cr-spinel seam petrogenesis in the Rum
788 Layered Suite, NW Scotland: cumulate assimilation and in situ crystallization in a deforming
789 crystal mush. Journal of Petrology. 51, 1171–1201.
790 O'Driscoll, B., González-Jiménez, J.M. 2016. Petrogenesis of the platinum-group minerals. Reviews in
791 mineralogy and geochemistry. Mineral. Soc. Am. 81, 489–578.
792 Pearson, D.G. 2005. Mantle Samples Included in Volcanic Rocks: Xenoliths and Diamonds, in:
793 Carlson, R.W. (ed.), The Mantle and Core. Treatise on Geochemistry.
794 Peate, D.W. 1997. The Paraná-Etendeka Province In: Mahoney, J.J. and Coffin, M.F. (ed.) Large
795 Igneous Provinces: Continental, Oceanic, and Planetary Flood Volcanism. 217-245.
796 Pitcher, L., Helz, R.T., Walker, R.J., Piccoli, P. 2009. Fractionation of the platinum-group elments and
797 Re during crystallization of basalt in Kilauea Iki Lava Lake, Hawaii. Chem. Geol. 260, 196–210.
798 https://doi.org/10.1016/j.chemgeo.2008.12.022.
799 Pohl, W.L. 2011. Economic geology: principles and practice, John Wiley & Sons.

800 Poulson, S.R. and Ohmoto, H. 1990. An evaluation of the solubility of sulfide sulfur in silicate melts
801 from experimental data and natural samples. Chemical Geology. 85, 57-75.
802 Ripley, E.M., Li, C. 2013. Sulfide saturation in mafic magmas: Is external sulfur required for magmatic
803 Ni-Cu-(PGE) ore genesis? Econ. Geol. 108, 45–58. https://doi.org/10.2113/econgeo.108.1.45.
804 Sauerzapf, U., Lattard, D., Burchard, M., Engelmann, R. 2008. The Titanomagnetite–Ilmenite
805 Equilibrium: New Experimental Data and Thermo-oxybarometric Application to the
806 Crystallization of Basic to Intermediate Rocks. Journal of Petrology. 49, 1161-1185.
807 Spandler, C., Mavrogenes, J. and Arculus, R. 2005. Origin of chromitites in layered intrusions: Evidence
808 from chromite-hosted melt inclusions from the Stillwater Complex. Geology. 33, 893–896.
809 Tegner, C. 1997. Iron in plagioclase as a monitor of the differentiation of the Skaergaard Intrusion.
810 Contributions to Mineralogy and Petrology. 128, 45-51.
811 Tornos, F., Velasco, F., Hanchar, J.M. 2016 Iron-rich melts, magmatic magnetite, and superheated
812 hydrothermal systems: The El Laco deposit, Chile. Geology. 44, 427-430.
813 Wykes, J.L., O'Neill, H.S.C., Mavrogenes, J.A. 2014. The effect of feo on the sulfur content at sulfide
814 saturation (SCSS) and the selenium content at selenide saturation of silicate melts. J. Petrol.
815 56, 1407–1424. https://doi.org/10.1093/petrology/egv041.

Table 1

Elements	D_i*	D_i	Ore grade	Concentration factor	Key minerals	Product	Uses	Notable mineralised LMI locations
Ni	1 - 10	500	0.5 - 3 wt.%	5 - 10 x mantle	Pentlandite	Metal	Steel, metals, alloys	Bushveld Complex (South Africa), Great Dyke (Zimbabwe), Monchegorsk (Russia), Stillwater (USA)
(Co)	1 - 10	45 - 80	0.05 - 0.1 wt.%		Pentlandite and other Ni,Fe- or Ni-sulphides			
(Cu)	< 0.1	1500	0.1 - 2 wt.%		Chalcopyrite			
(Au)	< 0.1	1000 - 10000	> 1 - 10 ppm	1000 x mantle	Electrum or alloys with PGE / metalloids, sulphides	Metal	Jewellery, electronics, finance, medicine	Bushveld Complex (South Africa), Skaergaard (Greenland)
PPGE	< 0.1	3000 - 500000	> 1 - 5 ppm total PGE	1000 x mantle	PGM and sulphides	Platinum-group metals	Catalytic converters, jewellery, electronics, fuel cells	Bushveld Complex (South Africa), Great Dyke (Zimbabwe), Monchegorsk (Russia), Stillwater (USA), Lac des Isles (Canada), Skaergaard (Greenland)
IPGE	1 - 10	2000 - 450000			PGM, chromite, sulphides			
Cr	< 0.1	10 - 100	20 - 50 % chromite: > 44 wt.% Cr_2O_3 for metallurgical uses, > 60 wt.% Al_2O_3 + Cr_2O_3 and > 20 wt.% Al_2O_3 for refractory uses.	20 - 60 x mantle	Chromite	Ferrochrome, chromium metal	Stainless steel, superalloys	Bushveld Complex (South Africa), Great Dyke (Zimbabwe), Kemi (Finland), Isle of Rum (Scotland)
V	< 0.1		~ 0.25 wt.% V_2O_5 in magnetite with > 50 % magnetite (low Ti)	25 - 160 x mantle	Magnetite	Titanium metal, TiO_2	White paint, metal (aerospace/automobile), chemicals, medicine, jewellery	Bushveld Complex (South Africa), Mustavaara (Finland), Panzhihua (China), Lac Doré Complex (Canada), Windimurra (Australia)
Ti	< 0.1		15 wt.% TiO_2 (equivalent to ~ 30 % ilmenite)	100 - 200 x mantle	Ilmenite	Ferrovanadium	Steel, chemicals, bonding agents, ceramics, magnets	

*D_i * is bulk partition coefficient between mantle minerals and silicate melt during partial melting of the mantle and under condition typical for the generation of basaltic magmas.*

D_i is partition coefficient into the typical phase which concentrates these elements (e.g., sulphide melt for chalcophile elements like Cu and the PGE; oxides for Cr, V and Ti).

PPGE is Pd-group platinum-group elements (Rh, Pt, Pd). IPGE is Ir-group platinum-group elements (Os, Ir, Ru). Here, PGM stands for platinum-group minerals.

Where elements are listed in brackets, indicates that these occur as co- or by-products to the main ores listed in this chapter. Information for elements in brackets therefore does not show the main ore locations.

Note that 1 ppm = 1 g/t

Figure 1

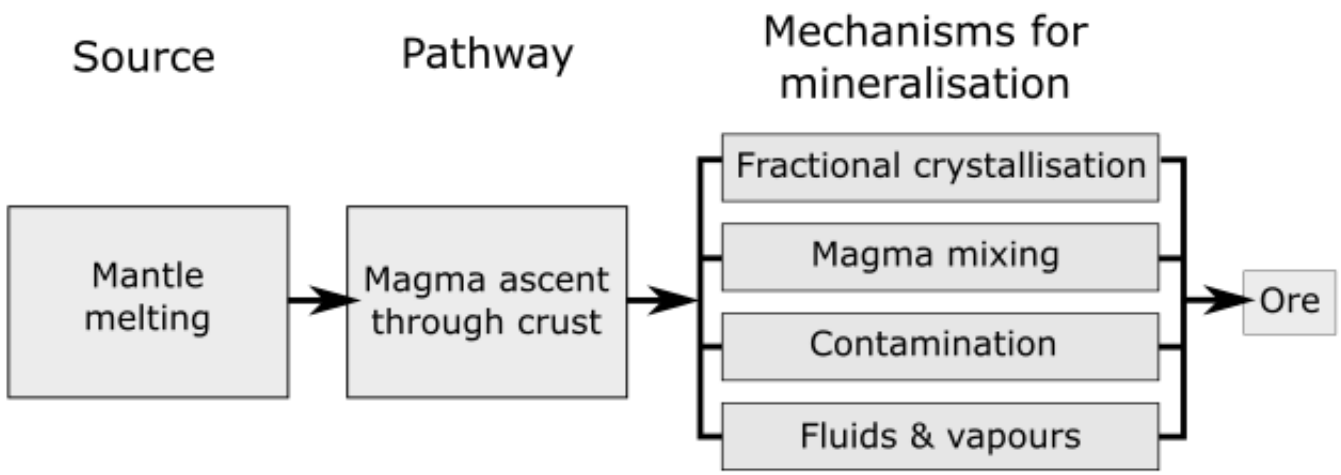
Source
Pathway
Mechanisms for mineralisation
Mantle melting
Magma ascent through crust
Fractional crystallisation
Magma mixing
Contamination
Fluids & vapours
Ore

Figure 2

(a)

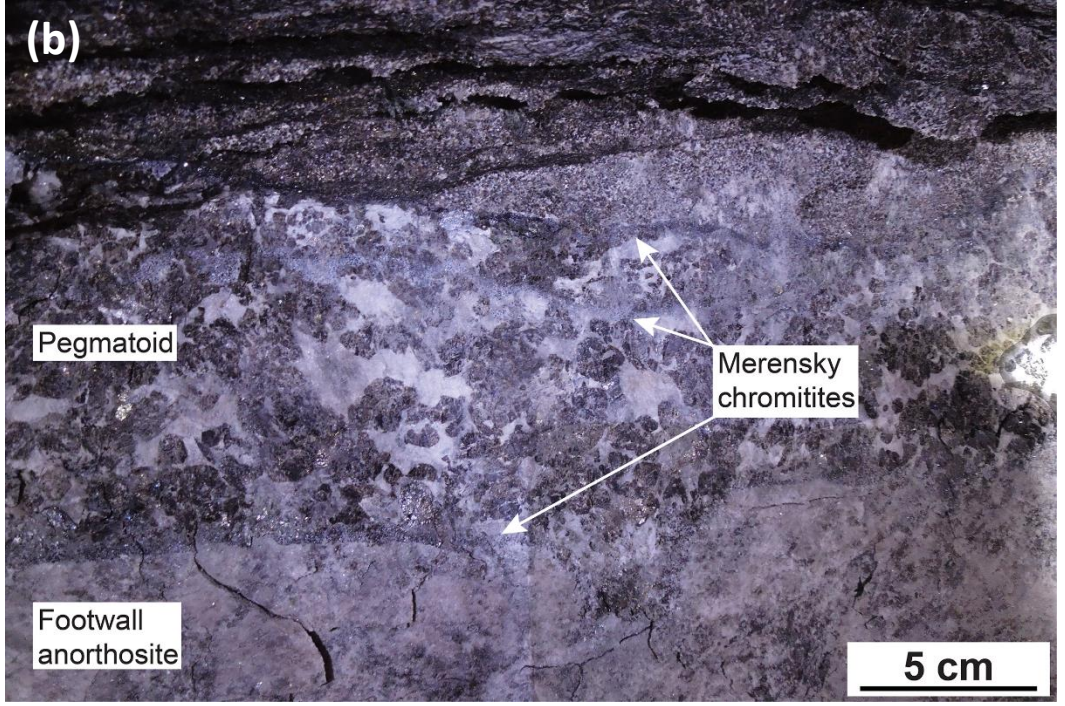
(b)
Pegmatoid
Merensky
chromitites
Footwall
anorthosite
5 cm

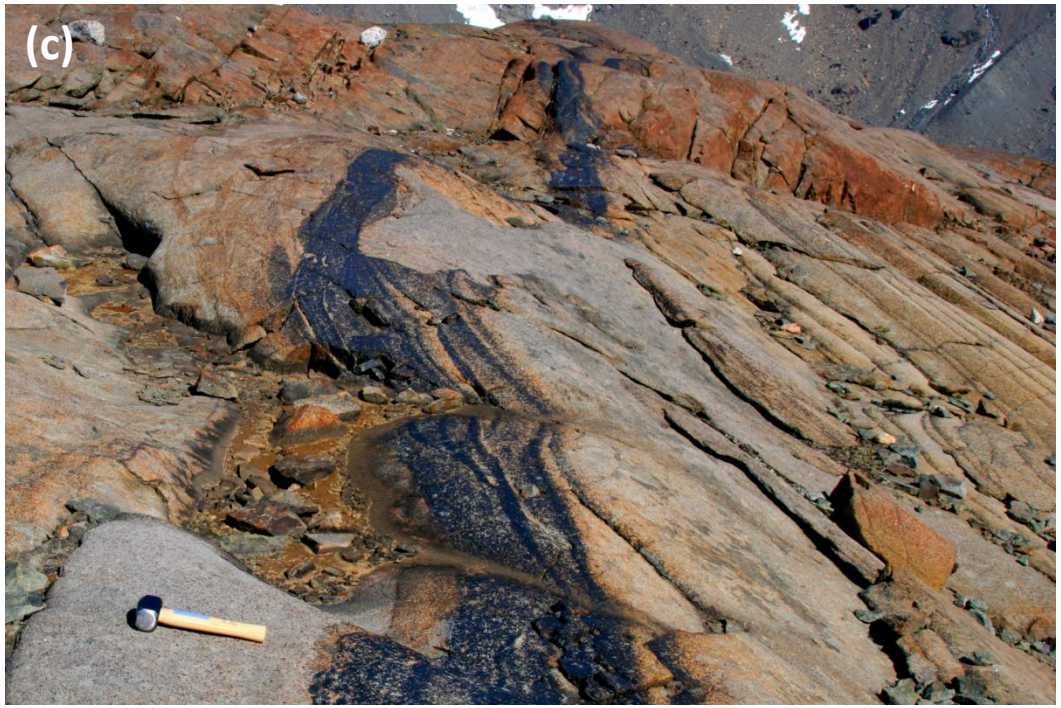
(c)

(d)

Figure 3

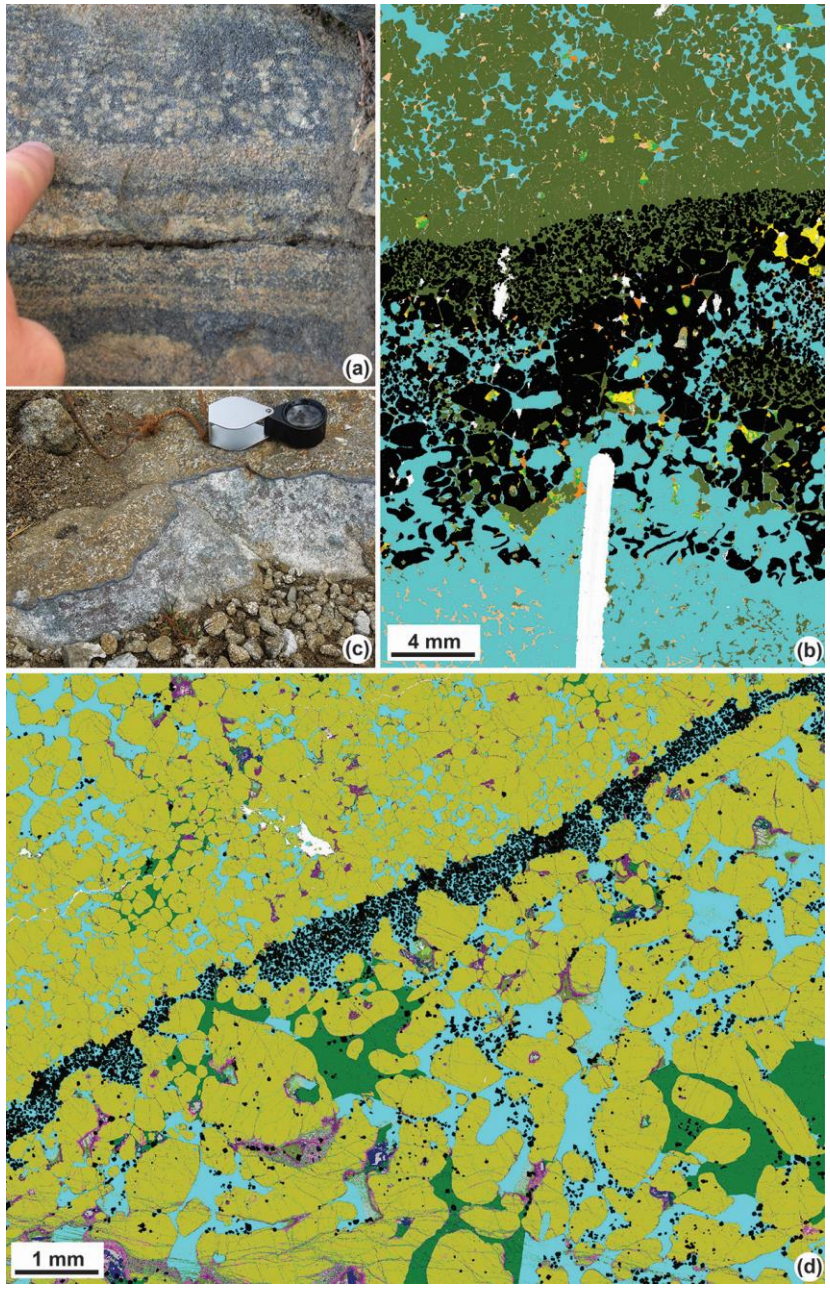

Figure 4

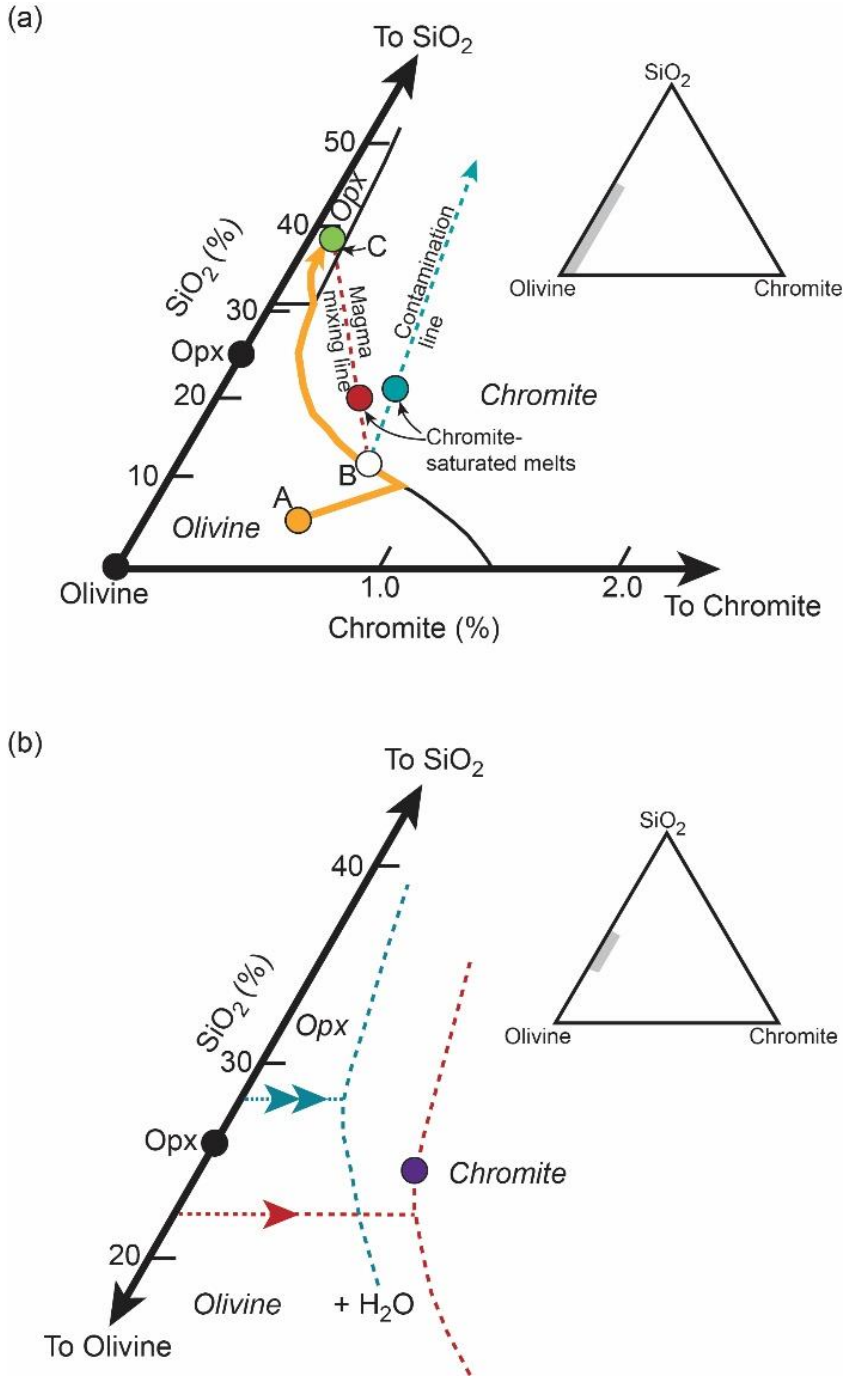
(a)
To SiO_2
50
40
30
20
10
SiO_2 (%)
Opx
C
Magma mixing line
Contamination line
Opx
Chromite
Chromite-saturated melts
B
A
Olivine
Olivine
1.0
2.0
To Chromite
Chromite (%)
SiO_2
Olivine
Chromite
(b)
To SiO_2
40
30
20
SiO_2 (%)
Opx
Opx
Chromite
Olivine
+ H_2O
To Olivine
SiO_2
Olivine
Chromite

Figure 5

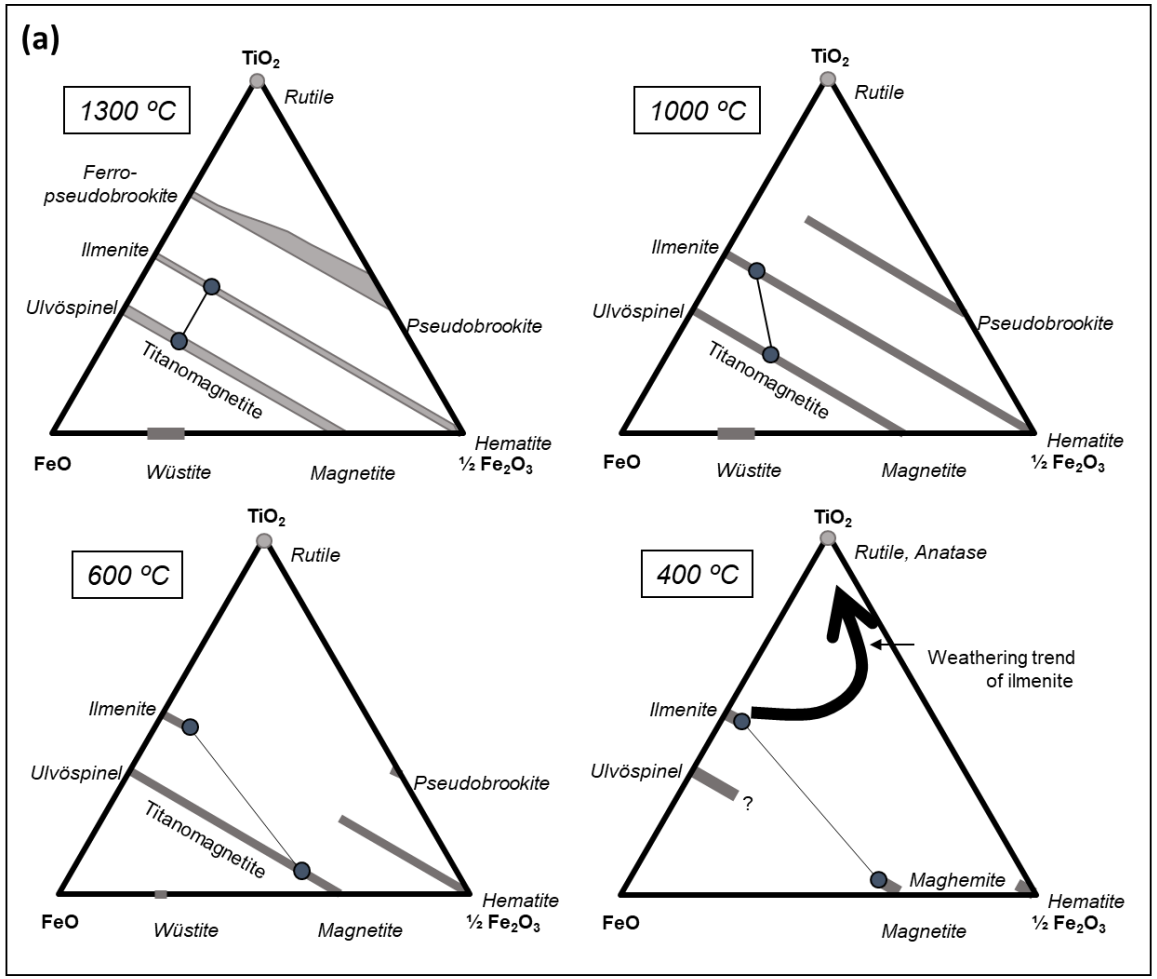
(a)
1300 ºC
TiO2
Rutile
Ferro-pseudobrookite
Ilmenite
Ulvöspinel
Pseudobrookite
Titanomagnetite
Hematite ½ Fe2O3
FeO
Wüstite
Magnetite
1000 ºC
TiO2
Rutile
Ilmenite
Ulvöspinel
Pseudobrookite
Titanomagnetite
Hematite ½ Fe2O3
FeO
Wüstite
Magnetite
600 ºC
TiO2
Rutile
Ilmenite
Ulvöspinel
Pseudobrookite
Titanomagnetite
Hematite ½ Fe2O3
FeO
Wüstite
Magnetite
400 ºC
TiO2
Rutile, Anatase
Weathering trend of ilmenite
Ilmenite
Ulvöspinel
?
Maghemite
Hematite ½ Fe2O3
FeO
Magnetite

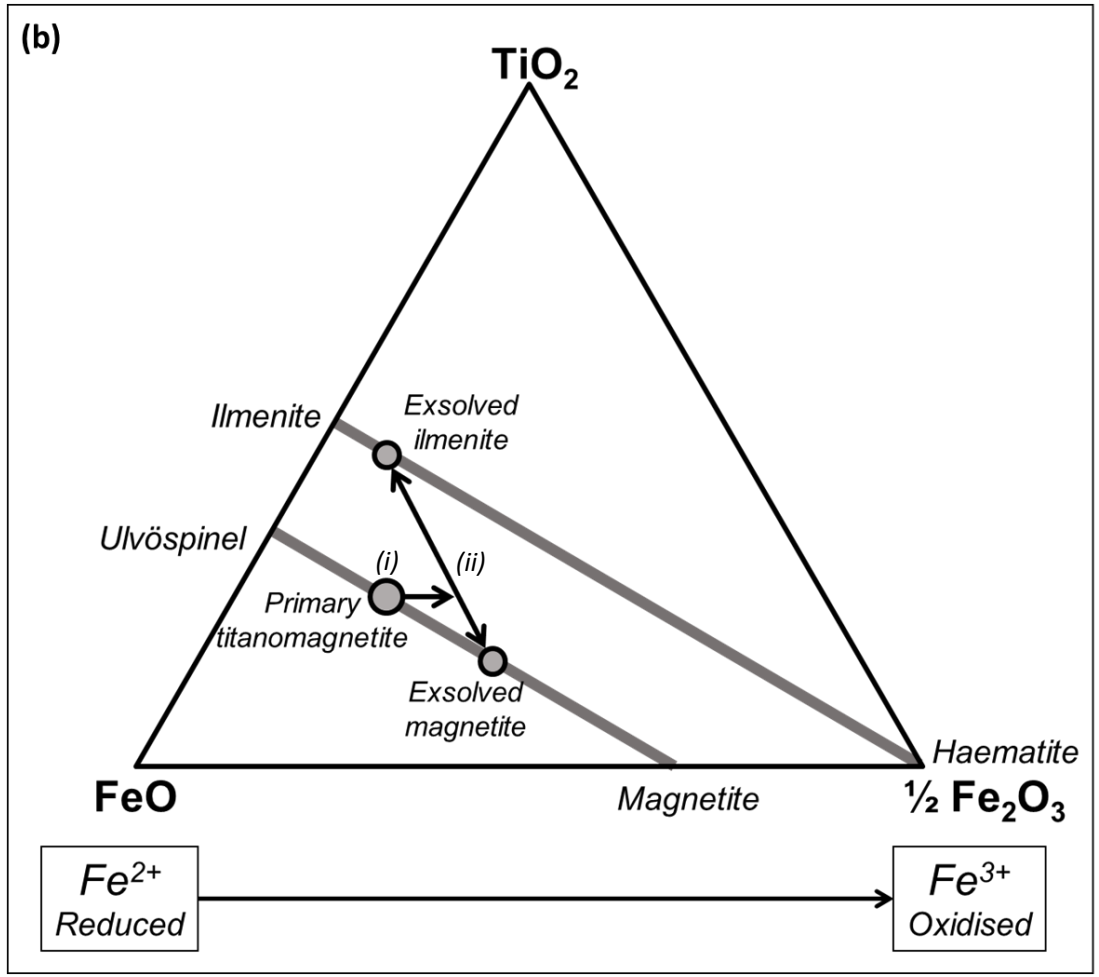
(b)
TiO2
Ilmenite
Exsolved ilmenite
Ulvöspinel
(i)
(ii)
Primary titanomagnetite
Exsolved magnetite
Haematite ½ Fe2O3
FeO
Magnetite
Fe2+ Reduced
Fe3+ Oxidised

Figure 6

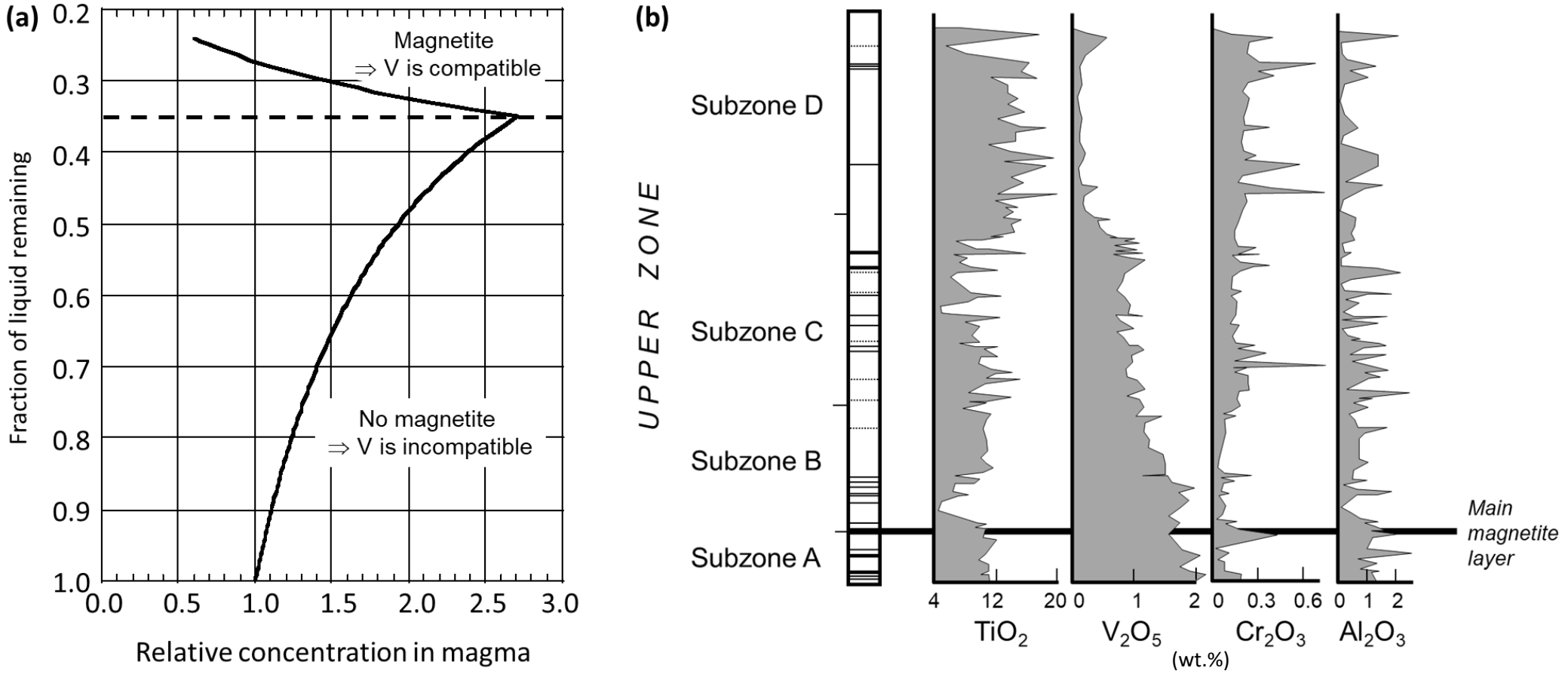
(a)
Magnetite
⇒ V is compatible
No magnetite
⇒ V is incompatible
Fraction of liquid remaining
0.2
0.3
0.4
0.5
0.6
0.7
0.8
0.9
1.0
0.0
0.5
1.0
1.5
2.0
2.5
3.0
Relative concentration in magma
(b)
UPPER ZONE
Subzone D
Subzone C
Subzone B
Subzone A
Main magnetite layer
4
12
20
0
1
2
0
0.3
0.6
0
1
2
TiO2
V2O5
Cr2O3
Al2O3
(wt.%)

Figure 7

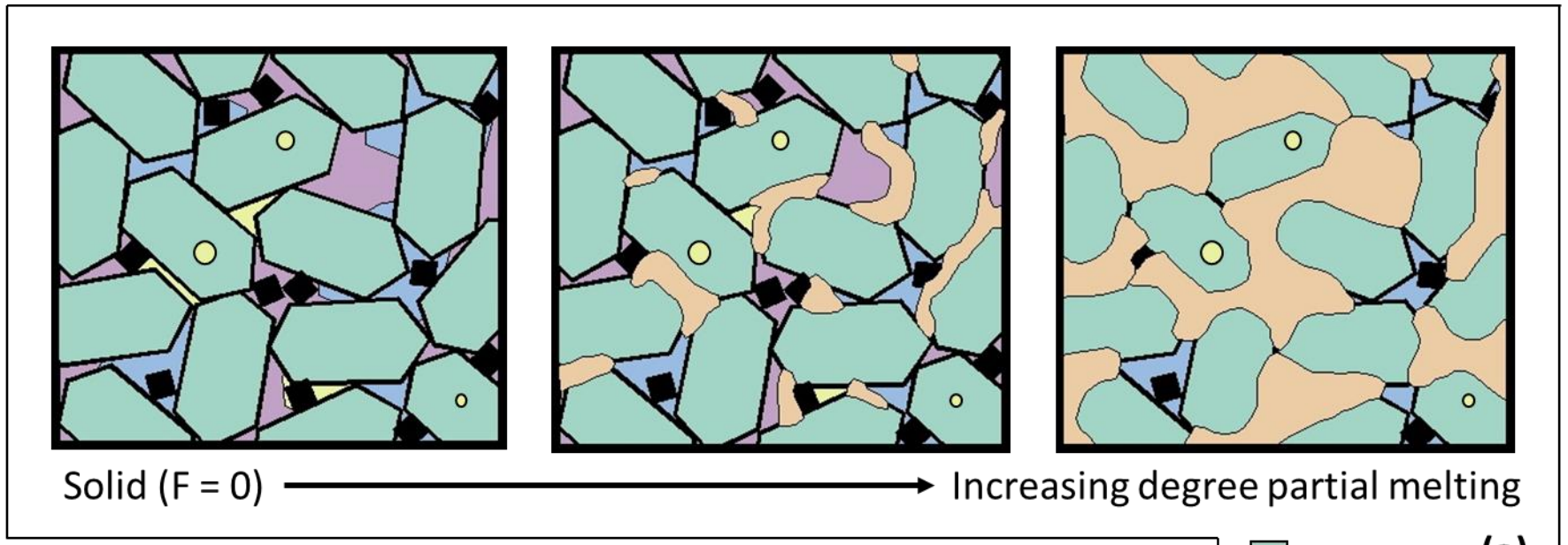
Solid (F = 0)
Increasing degree partial melting
(a)
Olivine
Orthopyroxene
Clinopyroxene
Sulphides
Chromite
Partial melt

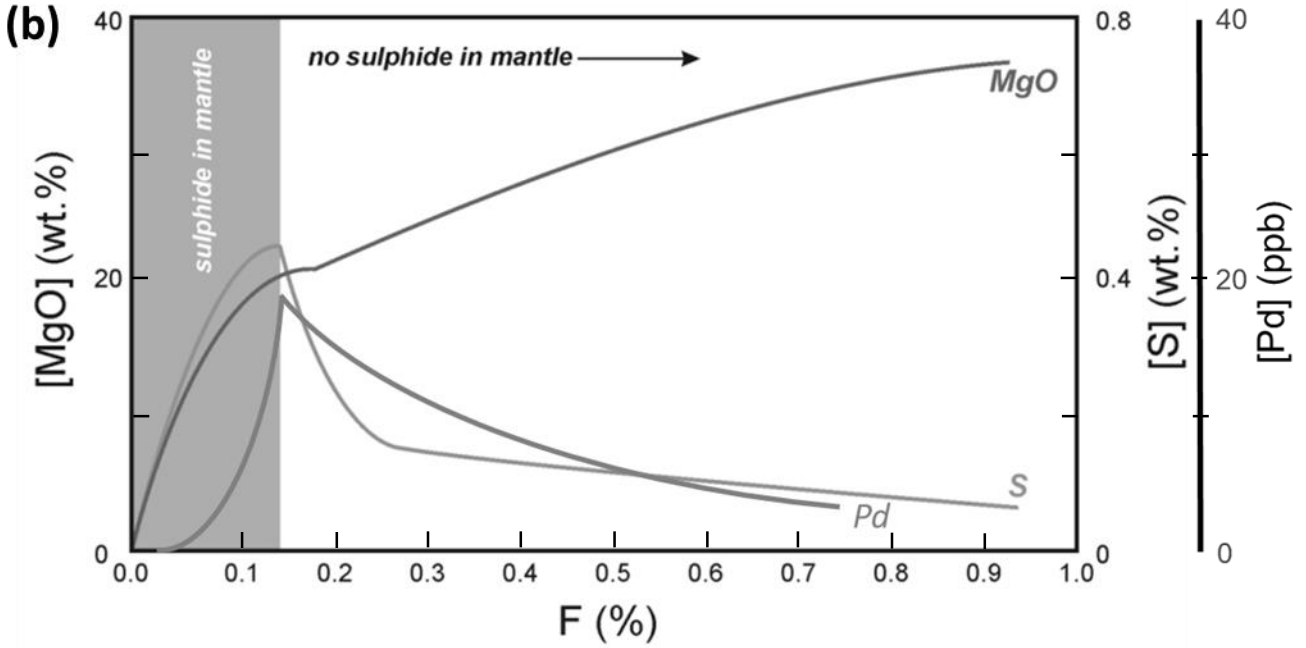
(b)
no sulphide in mantle
sulphide in mantle
MgO
S
Pd
[MgO] (wt.%)
[S] (wt.%)
[Pd] (ppb)
F (%)
0
20
40
0.4
0.8
0.0
0.1
0.2
0.3
0.4
0.5
0.6
0.7
0.8
0.9
1.0

Figure 8

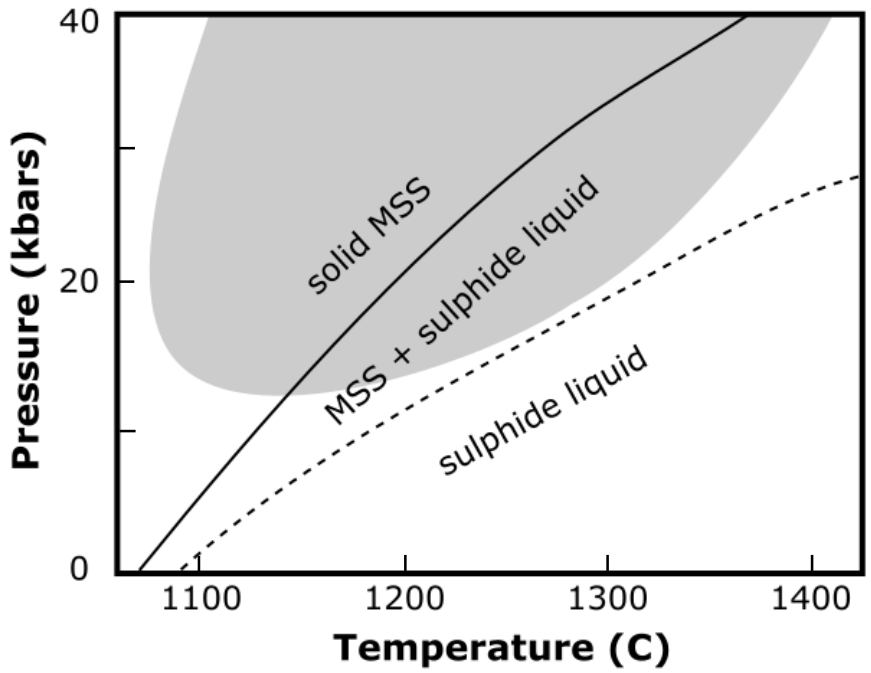
40
20
0
Pressure (kbars)
1100
1200
1300
1400
Temperature (C)
solid MSS
MSS + sulphide liquid
sulphide liquid

Figure 9

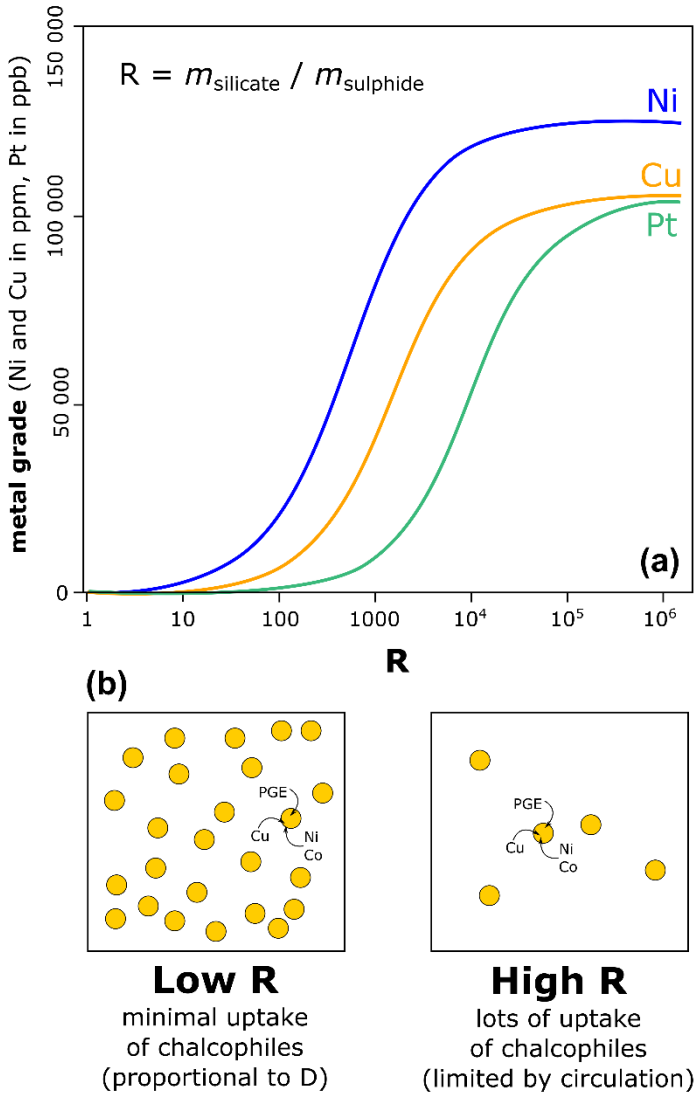
R = $m_{silicate}$ / $m_{sulphide}$
Ni
Cu
Pt
(a)
metal grade (Ni and Cu in ppm, Pt in ppb)
150 000
100 000
50 000
0
1
10
100
1000
10^4
10^5
10^6
R
(b)
PGE
Cu
Ni
Co
Low R
minimal uptake
of chalcophiles
(proportional to D)
High R
lots of uptake
of chalcophiles
(limited by circulation)

Figure 10

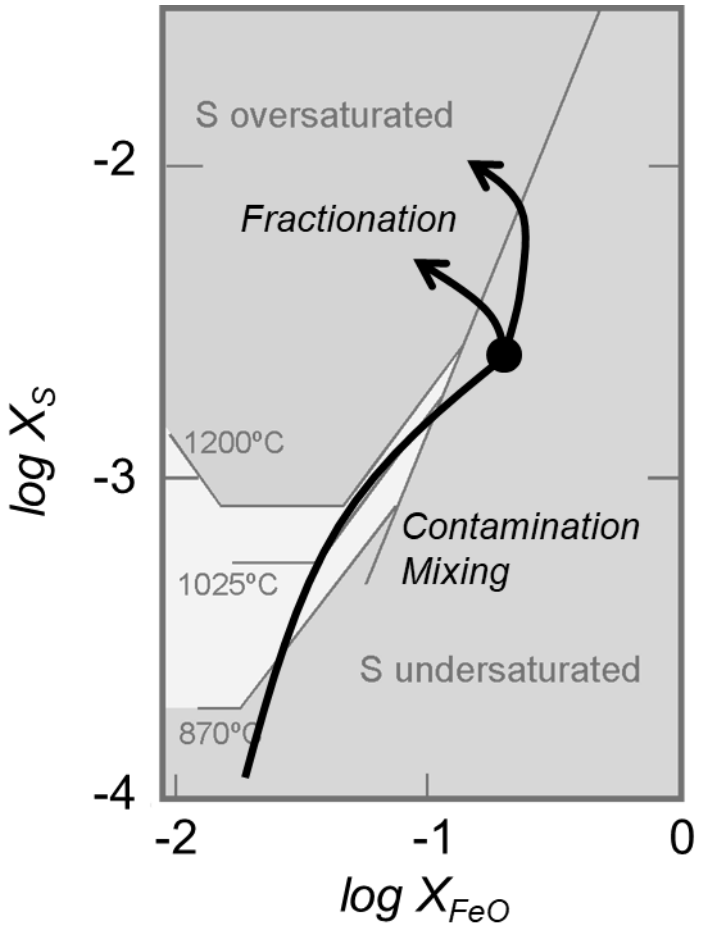
S oversaturated
Fractionation
1200°C
Contamination
Mixing
1025°C
S undersaturated
870°C
-2
-3
-4
-2
-1
0
log X_S
log X_{FeO}